Free Radical Biology and Medicine 213 (2024) 248–265

Contents lists available at ScienceDirect

Free Radical Biology and Medicine

journal homepage: www.elsevier.com/locate/freeradbiomed

Cardiomyocyte maturation alters molecular stress response capacities and determines cell survival upon mitochondrial dysfunction

Nina Schraps [a], Michaela Tirre [b], Simon Pyschny [b], Anna Reis [c], Hannah Schlierbach [d], Matthias Seidl [e], Hans-Gerd Kehl [b], Anne Schänzer [d], Jacqueline Heger [c], Christian Jux [a,b], Jörg-Detlef Drenckhahn [a,b,*]

[a] Department of Pediatric Cardiology, Justus Liebig University, Gießen, Germany
[b] Department of Pediatric Cardiology, University Hospital Münster, Münster, Germany
[c] Institute of Physiology, Justus Liebig University, Gießen, Germany
[d] Institute of Neuropathology, Justus Liebig University, Gießen, Germany
[e] Institute of Pharmacology and Toxicology, Westfälische Wilhelms University, Münster, Germany

ARTICLE INFO

Keywords:
Cardiomyocyte survival
Oxidative stress
Mitochondrial dysfunction
Cardiomyocyte differentiation
Cellular stress response

ABSTRACT

Cardiomyocyte maturation during pre- and postnatal development requires multiple intertwined processes, including a switch in energy generation from glucose utilization in the embryonic heart towards fatty acid oxidation after birth. This is accompanied by a boost in mitochondrial mass to increase capacities for oxidative phosphorylation and ATP generation required for efficient contraction. Whether cardiomyocyte differentiation is paralleled by augmented capacities to deal with reactive oxygen species (ROS), physiological byproducts of the mitochondrial electron transport chain (ETC), is less clear. Here we show that expression of genes and proteins involved in redox homeostasis and protein quality control within mitochondria increases after birth in the mouse and human heart. Using primary embryonic, neonatal and adult mouse cardiomyocytes in vitro we investigated how excessive ROS production induced by mitochondrial dysfunction affects cell survival and stress response at different stages of maturation. Embryonic and neonatal cardiomyocytes largely tolerate inhibition of ETC complex III by antimycin A (AMA) as well as ATP synthase (complex V) by oligomycin but are susceptible to complex I inhibition by rotenone. All three inhibitors alter the intracellular distribution and ultrastructure of mitochondria in neonatal cardiomyocytes. In contrast, adult cardiomyocytes treated with AMA undergo rapid morphological changes and cellular disintegration. At the molecular level embryonic cardiomyocytes activate antioxidative defense mechanisms, the integrated stress response (ISR) and ER stress but not the mitochondrial unfolded protein response upon complex III inhibition. In contrast, adult cardiomyocytes fail to activate the ISR and antioxidative proteins following AMA treatment. In conclusion, our results identified fundamental differences in cell survival and stress response in differentiated compared to immature cardiomyocytes subjected to mitochondrial dysfunction. The high stress tolerance of immature cardiomyocytes might allow outlasting unfavorable intrauterine conditions thereby preventing fetal or perinatal heart disease and may contribute to the regenerative capacity of the embryonic and neonatal mammalian heart.

1. Introduction

Mitochondria are critically important for cardiovascular health and disease by affecting growth, survival and function of different myocardial cell types. Consequently, mitochondrial dysfunction is involved in various cardiac pathologies including ischemia/reperfusion injury, drug induced cardiotoxicity, cardiomyopathy as part of syndromic mitochondrial diseases as well as cardiac ageing [1,2]. Constantly contracting cardiomyocytes in particular rely on intact mitochondria considering their involvement in multiple metabolic processes (including the TCA cycle, β-oxidation of fatty acids or anaplerosis), energy generation, redox homeostasis, cell death as well as calcium handling [3].

Along with progressing cardiomyocyte differentiation mitochondria

* Corresponding author. Department of Pediatric Cardiology, Justus Liebig University Gießen, Feulgenstraße 10-12, Gießen, Germany.
E-mail address: Joerg.Drenckhahn@paediat.med.uni-giessen.de (J.-D. Drenckhahn).

https://doi.org/10.1016/j.freeradbiomed.2024.01.034
Received 29 November 2023; Received in revised form 11 January 2024; Accepted 21 January 2024
Available online 22 January 2024

undergo metabolic and structural maturation during pre- and postnatal heart development [4,5]. Whereas immature cardiomyocytes contain a relatively low number of small and circular or elliptical mitochondria with loosely organized cristae, a burst of mitochondrial biogenesis after birth accompanied by fusion events results in an extended network of elongated mitochondria with complex folding of the inner mitochondrial membrane resulting in dense cristae structures. Along with structural changes cardiac mitochondria undergo substantial metabolic adaptations after birth. Whereas cardiomyocytes in the embryonic and fetal heart primarily rely on aerobic glycolysis for ATP generation, postnatal and adult cardiomyocytes switch to an oxidative metabolisms primarily fueled by fatty acids [4–6]. This increase in mitochondrial β-oxidation has been shown to elevate the levels of reactive oxygen species (ROS) in the heart shortly after birth thereby activating a DNA damage response which contributes to postnatal cardiomyocyte cell cycle arrest [7].

Physiological ROS production along the mitochondrial respiratory chain can result in oxidation of lipids, DNA and proteins [2,3,8]. Oxidative damage impairs function of existing proteins and causes misfolding of newly synthesized proteins which eventually form aggregates within different cellular compartments. Therefore, cells harbor complex protein quality control (PQC) machineries aiming at proper folding of newly synthesized proteins, refolding of damaged proteins, resolving aggregates and degrading irreversibly damaged proteins [9,10]. The latter include an organelle specific unfolded protein response (UPR) which leads to translational inhibition to prevent further synthesis of misfolded proteins. In addition, the UPR regulates protein folding capacity by increasing the expression of chaperones and at the same time inducing proteases to allow degradation of damaged and aggregated proteins [9,10]. The UPR partially overlaps with the integrated stress response (ISR), a joint effector pathway activated by various upstream mechanisms which converge on the phosphorylation of eIF2α (eukaryotic translation initiation factor 2A) [11]. This generally causes translational inhibition whereas a subset of mRNAs containing specific upstream open reading frames is preferentially translated. Among the latter is ATF4 (activating transcription factor 4), a core transcription factor of the ISR and UPR which induces genes involved in PQC [9–11]. Another PQC mechanism is the heat shock response (HSR), which mainly regulates chaperone expression upon accumulation of misfolded proteins [12]. Furthermore, cells harbor an extensive network of proteins and enzymes involved in scavenging ROS thereby preventing oxidative damage of macromolecules. This ROS detoxification involves enzymes such as superoxide dismutase, peroxiredoxin, catalase and thioredoxin [13]. The expression, activity and interaction of these components are essential to maintain intracellular redox homeostasis and prevent oxidative stress.

Whether embryonic and adult cardiomyocytes rely on different mechanisms of PQC or redox homeostasis to cope with physiological ROS production is incompletely understood. Moreover, mitochondrial dysfunction usually results in markedly increased ROS levels eventually leading to oxidative stress induced cell death [1–3]. Whether the outcome of such pathological conditions in the heart depends on the state of cardiomyocyte differentiation is not clear. However, understanding stress tolerance of embryonic, fetal and neonatal cardiomyocytes is highly relevant for the pathogenesis of congenital heart disease as insults during intrauterine or perinatal development might impair cell survival, growth and differentiation thereby affecting cardiac morphogenesis and heart function [14]. In contrast, a potential loss of stress tolerance upon terminal differentiation might identify new therapeutic targets for cardioprotection in the adult heart by reactivating embryonic stress response mechanisms [15]. The current study investigated the consequences of mitochondrial dysfunction in primary embryonic, neonatal and adult mouse cardiomyocytes in vitro. Furthermore, we evaluated RNA and protein expression of multiple genes involved in UPR/ISR, HSR and redox homeostasis throughout pre- and postnatal heart development in mice and humans. The results highlight remarkable differences in stress tolerance and survival of immature compared to differentiated cardiomyocytes and might therefore help to better understand the impact of mitochondrial dysfunction on the pathogenesis of pre- and postnatal cardiovascular disease.

2. Material and methods

2.1. Isolation and culture of embryonic and neonatal mouse cardiomyocytes

All animal procedures including the preparation of embryonic, fetal, neonatal and adult mouse hearts have been approved by institutional (JLU approval number 702_M) or governmental (RP Giessen approval number GI 20/12 Nr. G 49/2017 and G 47/2020) authorities and were performed according to Directive 2010/63/EU of the European Parliament on the protection of animals used for scientific purposes. C57BL/6J mice (purchased from Charles River) were used for primary cardiomyocyte isolation. Embryonic hearts were harvested at 12.5–14.5 dpc (days post conception). Pregnant dams were sacrificed by cervical dislocation, embryos were dissected in cold PBS and sacrificed by decapitation. Hearts were prepared and atria and outflow tract were removed such that mainly ventricular myocardium was used for cell dissociation. Neonatal mice were sacrificed by decapitation on day 1–2 after birth, hearts were dissected in cold PBS and atria were removed. Tissue was dissociated using the gentleMACS™ Octo Dissociator with Heaters and the Neonatal Heart Dissociation Kit for mouse and rat (Miltenyi Biotec) according to the manufacturer's instructions. All hearts from one preparation were pooled (usually 15–20 embryonic or 8–10 neonatal hearts). Cells were seeded at a density of approximately 70.000 cells/cm^2 in 8-well chamber slides, 12-well or 6-well plates. Culture dishes had previously been coated with 5 μg/ml laminin (L2020, Sigma Aldrich) in PBS at 37°C over-night. Embryonic and neonatal cardiomyocytes were cultured in DMEM (D6429) supplemented with non-essential amino acids (M7145), 10% fetal bovine serum (F7524, all components from Sigma Aldrich) and 1% penicillin/streptomycin (BS.A 2213, Bio&SELL) at 37°C with 95% air and 5% CO_2. Cells were allowed to recover over-night before treatment in culture medium with the following compounds (final concentrations are provided in figure legends): Antimycin A (A8674), Rotenone (R8875), Oligomycin (O4876, all from Sigma Aldrich), DMSO (A3672, AppliChem).

2.2. Isolation and culture of adult mouse cardiomyocytes

Mice aged between 3 and 6 months were anaesthetized by inhalation of 5% isoflurane followed by euthanasia by cervical dislocation. The hearts were extracted and rinsed with 4°C cold 0.9% NaCl solution. Thereafter, the hearts were digested with retrograde perfusion in a Langendorff apparatus for 25 min at 37°C in a calcium-free buffer (10 mM Glucose, 25 mM HEPES, 2.5 mM KCl, 1.2 mM KH_2PO_4, 1.2 mM $MgSO_4$, 110 mM NaCl, pH 7.4) containing 2.4 mg/ml collagenase and supplemented with 1 mM BDM (butanedione monoxime, B0753, Sigma Aldrich). Subsequently, atria and outflow tract were removed and the remaining ventricular myocardium was minced and incubated for another 5 min in the digestion buffer. Cell dissociation was supported by pipetting, the suspension was filtered through a nylon mesh (200 μm pore size) and the cardiomyocytes were separated from other cells by centrifugation (20×*g* for 1 min). To gradually reconstitute the physiological calcium concentration the cells were centrifuged and resuspended with a step-wise increase of calcium (125 μM, 250 μM, 500 μM, 1 mM in perfusion buffer) followed by a final resuspension in maintenance buffer (2.5 mM $CaCl_2$-dihydrate, 5 mM Glucose, 10 mM HEPES, 4.7 mM KCl, 1.2 mM KH_2PO_4, 0.8 mM $MgSO_4$, 118 mM NaCl, 1.9 mM Na-Pyruvate, pH 7.4). For short term experiments treatment of adult cardiomyocytes usually commenced on the same day of isolation. Cardiomyocytes were plated in maintenance buffer on laminin-coated culture dishes and incubated at 37°C (5.5% CO_2, 95% humidity) for 1.5 h to

allow adherence. Subsequently, maintenance buffer containing DMSO or AMA was added and incubated for the desired time.

For long term experiments after calcium reconstitution the cardiomyocytes were transferred to plating medium (MEM Eagle with HBSS (BE12-127F, Lonza), 10% FBS, 2 mM glutamine, 2 mM ATP, 10 mM BDM, 1% penicillin/streptomycin), plated on laminin-coated culture dishes and incubated at 37°C (5% CO_2, 95% humidity). After 1.5 h the medium was changed to culture medium (MEM Eagle with HBSS, 0.1% BSA, 2 mM glutamine, 10 mM BDM, 1% penicillin/streptomycin, supplemented with ITS (Insulin-Transferrin-Selenium, I1884, Sigma Aldrich)) and cells were kept over-night before treatment in culture medium.

2.3. Evaluation of cell viability and contractility

Cell density, viability, adherence, morphology and cardiomyocyte contractility were evaluated by phase-contrast microscopy and imaged using a Zeiss Axio Observer 7 microscope. To quantitatively assess contractility of embryonic and neonatal cardiomyocytes, short movies of ~20 s duration were recorded using a 10x N-Achroplan objective, an Axiocam 305 camera and ZEN 2.3 software (Zeiss). For embryonic cardiomyocytes 4 movies per well were recorded at random positions in 4 wells per treatment condition from two independent experiments (8 wells per treatment in total). Movies were superimposed with a 10x10 grid in the ZEN 2.3 software. Each square was evaluated for visible contraction and the number of squares with contraction was counted for each movie or microscopic field, respectively, and averaged from the four movies per well. For neonatal cardiomyocytes 2 movies in 4 wells per treatment were recorded and scored as described. In addition, in 5 areas per movie the frequency of spontaneous contraction was determined as beats per minute (bpm).

2.4. Immunofluorescence staining

For immunofluorescence staining embryonic cardiomyocytes were cultured in 8-well chamber slides (94.6140.802, Sarstedt) or 12-well plates on glass coverslips coated with laminin (L2020, Sigma Aldrich). After treatment with ETC inhibitors for the desired time (usually 24 h) culture medium was aspirated. Cells were washed twice in PBS for 2 min, fixed in 4% PFA in PBS for 10 min and permeabilized in PBS containing 0.25% Triton X-100 for 10 min (all steps at RT). After three washes in PBS for 5 min each blocking was performed in antibody solution (1% BSA, 0.1% Triton X-100, 0.05% Tween 20, 0.05% sodium azide in PBS) containing 5% normal goat serum (Jackson ImmunoResearch) for 1 h at RT, after which cells were incubated over night with primary antibodies at 4°C on a rocking platform. The following primary antibodies were used: Ki67 (14-5698-82, Thermo Fisher, 1:500), ATF4 (#11815, Cell Signaling Technology, 1:200), ATF5 (ab184923, Abcam, 1:500), cleaved caspase-3 (#9661, Cell Signaling, 1:400), Nkx2.5 (sc-14033, Santa Cruz, 1:500), α-Actinin (A7811, Sigma Aldrich, 1:800), SOD2 (24127-1-AP, Proteintech, 1:200), HSP60 (#4870, Cell Signaling, 1:1000). Secondary antibody detection was performed at room temperature for 1 h using Alexa Fluor 488, 555 or 647 conjugated secondary antibodies (A21434, A11029, A11008, A21428, A21247, Thermo Fisher, 1:500). Nuclei were stained with DAPI (#6335, Carl Roth) and cells were mounted in ProLong Gold antifade reagent (Cell Signaling Technology). Imaging was performed using a Zeiss Axio Observer 7 equipped with the ZEN 2.3 pro imaging capture software.

2.5. ROS detection

Reactive oxygen species were detected using the fluorescence probe MitoSOX Red (M36008, Thermo Fisher) according to the manufacturer's instructions. For fluorescence microscopy of MitoSOX cells were seeded in 8-well chamber slides (94.6140.802, Sarstedt) and treated with DMSO or antimycin A for 24 h. Medium was aspirated and 5 μM MitoSOX in DMEM was added in a total volume of 500 μl per well for 20 min at 37°C. Cells were washed two times in PBS and imaged using a 20x LD A-Plan objective (Zeiss).

2.6. Evaluation of cell size

To measure the surface area embryonic or neonatal cardiomyocytes were cultured in 8-well chamber slides and treated with DMSO or inhibitors of mitochondrial respiration for 24 h. Subsequently, immunofluorescence staining for α-actinin was performed as described above to outline cell borders. Imaging was performed using a 20x Plan-Apochromat objective on a Zeiss Axio Observer 7 microscope equipped with the ZEN 2.3 pro imaging capture software. Single α-actinin positive cardiomyocytes in loosely confluent areas with clearly discernible cell borders were selected and cell surface area was measured using ZEN blue software. The mean surface area of 30–40 cardiomyocytes per well was determined with $n = 4$ wells per culture condition.

2.7. Evaluation of cardiomyocyte purity and cell cycle activity

Cell cycle activity was assessed based on immunofluorescence staining for Ki67. Embryonic cardiomyocytes were cultured in 8-well chamber slides and treated with DMSO, antimycin A or oligomycin for 24 h. Subsequently, immunofluorescence staining for Ki67 and Nkx2.5 (to identify cardiomyocyte nuclei) was performed as described above. Four to six random fields per well were imaged using a Zeiss Axio Observer 7 fluorescence microscope and a 10x N-Achroplan objective. DAPI stained nuclei were counted using the "Find Maxima" function in ImageJ (https://imagej.net/ij/) with manual correction if required whereas Ki67 and Nkx2.5 positive nuclei were counted manually. The number of Nkx2.5 positive nuclei was subtracted from the total number of nuclei to reveal the number of non-myocyte nuclei. Similarly, the number of Ki67/Nkx2.5 double positive nuclei (indicating cycling cardiomyocytes) was subtracted from the total number of Ki67 nuclei to reveal the number of cycling non-myocytes. The percentage of Ki67 positive cardiomyocyte and non-myocyte nuclei was calculated for each image and averaged per well. Each culture condition was analyzed in triplicates, such that data was averaged from three wells.

In a second approach Ki67 staining was combined with α-actinin to identify cardiomyocytes. Embryonic and neonatal cardiomyocytes were cultured and treated as described. Twenty random fields per well were imaged using a 20x Plan-Apochromat objective. The total number of DAPI stained nuclei was counted using the Image Analysis Toolkit in the ZEN software (Zeiss). The number of cardiomyocyte nuclei located within α-actinin positive cells was counted manually and subtracted from the total number of nuclei to reveal non-myocyte nuclear numbers. Ki67 signals were counted manually and assigned to cardiomyocytes or non-myocytes based on α-actinin staining. The percentage of Ki67 positive cardiomyocyte and non-myocyte nuclei was calculated per well and averaged for each culture condition.

2.8. Evaluation of cell death

Programmed cell death (apoptosis) was detected by immunofluorescence staining for cleaved caspase-3 as described above including co-staining for α-actinin to differentiate cardiomyocytes and non-myocytes. Twenty random fields per well were imaged using a 20x Plan-Apochromat objective. The total number of DAPI stained nuclei was counted using the Image Analysis Toolkit in the ZEN software (Zeiss). The number of cardiomyocyte nuclei located within α-actinin positive cells was counted manually and subtracted from the total number of nuclei to reveal non-myocyte nuclear numbers. Cleaved caspase-3 signals were counted manually and assigned to cardiomyocytes or non-myocytes based on α-actinin staining. The percentage of apoptotic cardiomyocytes and non-myocytes was calculated per well and averaged

for each culture condition.

To determine cellular disintegration and necrosis in adult cardiomyocytes the release of lactate dehydrogenase into the culture medium was measured using the LDH Cytotoxicity Assay Kit from Cayman Chemical (#601170). Cells were seeded in 12-well plates for 24 h followed by antimycin A treatment with equivalent volumes of DMSO serving as control. Culture medium was collected at different time points after initiation of treatment. 100 µl of cell culture supernatant was used for the assay which was performed in white opaque 96-well flat-bottom microplates according to the manufacturer's instructions. Absorbance at 490 nm was measured in a CLARIOstar microplate reader (BMG Labtech) after 90 min. Three to four different wells per condition were analyzed and measurements were performed in duplicate for each well. Cell culture medium not in contact with any cells was included in the assay such that its absorbance was subtracted for blank correction.

2.9. Transmission electron microscopy

Neonatal mouse cardiomyocytes were isolated, cultured and treated with DMSO, antimycin A or oligomycin in 6-well plates for 24 h as described above. Cells were briefly washed in PBS and carefully detached using TrypLE Express (Gibco) at 37°C for approximately 15 min. Detachment was closely monitored and supported by gentle shaking and pipetting. Detachment was stopped by adding culture medium containing 10% FCS, cells were centrifuged at 200×*g* for 5 min and washed twice in PBS. After the final centrifugation the cell pellets were carefully overlayed with 2.9% glutaraldehyde in 0.4 M PBS (pH 7.2) without dissociating the cells and kept at 4°C for at least 4 h. The cell pellets were washed in 0.1 M PBS (pH 7.2) and were transferred to 1% osmium tetroxide (OsO_4) in Aqua dest. The cell pellets were dehydrated in ascending grades of ethanol (25, 35, 50, 70, 75, 85 and 3 × 100%) for 10 min each. The second and third incubations in 100% ethanol were extended to 20 min. The cell pellets were then dehydrated in propylene oxide and a propylene oxide/resin mixture (1:1) for 20 min each and after that infiltrated with a resin mixture and kept in a desiccator overnight. Polymerization of the resin was accomplished in an oven at 60°C for 24 h. Semi-thin sections (990 nm thickness) were prepared and stained with 1% Richardson to assess overall cell morphology. Ultrathin sections (190 nm thickness) were prepared and mounted on copper grids. Ultrathin sections were contrasted with uranyless and 3% lead citrate with a Leica EM AC20. The contrasted ultrathin sections were examined and photographed using a Zeiss EM 109 transmission electron microscope equipped with a Slowscan 2 K-CCD digital camera (2K wide angel sharp:eye). Only cardiomyocytes with clearly visible sarcomeric structures were analyzed for mitochondrial pathology. At least 10 cells per pellet were observed from two independent pellets per treatment. Cells with morphological alterations like sarcomeric hypercontraction, membrane rupture or increased numbers of vacuoles were excluded.

2.10. Isolation of proteins from murine hearts

Mice on a mixed 129Sv/C57BL/6 genetic background were used for protein isolation. Pregnant mice were sacrificed by cervical dislocation at 13.5 dpc or 16.5 dpc and embryos/fetuses were dissected from the uterus directly into ice cold PBS followed by decapitation. Newborn mice were sacrificed by decapitation on postnatal day 1 and adult mice were sacrificed by cervical dislocation at the age of 8 weeks. For embryos, fetuses and neonates the entire heart (including atria and outflow tract) was prepared and snap frozen in liquid nitrogen whereas the apex was used for adult hearts. For isolation of cardiac proteins embryonic and fetal hearts were homogenized using micro pestles in RIPA buffer supplemented with protease (Complete Protease Inhibitor Cocktail Tablets, Roche Diagnostics) and phosphatase (PhosSTOP Phosphatase Inhibitor Cocktail Tablets, Roche) inhibitors. Neonatal and adult heart tissue was homogenized using a Precellys Evolution Homogenizer (Bertin Technologies). The tissue lysates were subsequently incubated at 4°C for 2 h with gentle agitation and centrifuged at 12.000×*g* for 10 min at 4°C. Protein concentration in the supernatant was determined by a modified Lowry assay (DC Protein Assay, BIO-RAD). Per sample 20 µg of protein was used for Western blot analyses.

2.11. Western blot analyses

For protein isolation embryonic and adult cardiomyocytes were cultured in 6-well plates and treated as desired. Cells were washed in PBS and lysed in 50 µl cell lysis buffer (#9803, Cell Signaling Technology) supplemented with protease (Complete Protease Inhibitor Cocktail Tablets, Roche Diagnostics) and phosphatase (PhosSTOP Phosphatase Inhibitor Cocktail Tablets, Roche) inhibitors for 10 min on ice. Cells were mechanically disrupted using cell scrapers, the lysate was transferred to a reaction tube and centrifuged at 12.000×*g* for 10 min at 4°C. Protein concentration in the supernatant was determined by a modified Lowry assay (DC Protein Assay, BIO-RAD). For samples on the same gel equal protein amounts (usually 10–20 µg) were loaded, separated by denaturing polyacrylamide gel electrophoresis (SDS-PAGE) and blotted onto nitrocellulose membranes (GE Healthcare). Membranes were blocked for 1 h in 5% non-fat dry milk (Carl Roth) in TBS-T and incubated with primary antibodies at 4°C over night. A list of primary antibodies used in this study is provided in Supplementary Table S1. Antibodies against GAPDH, α-Tubulin and Vinculin were used for loading control and for normalization upon densitometric quantifications. Secondary detection was performed using horseradish peroxidase (HRP)-linked secondary antibodies (Cell Signaling, #7074 and #7076, 1:2000). Standard enhanced chemiluminescence (ECL) reaction was used for abundant proteins whereas weakly expressed proteins were detected using the SuperSignal West Femto Maximum Sensitivity Substrate (Thermo Scientific). ECL signals were imaged with a Vilber Lourmat Fusion Solo 6 S Edge or ChemiDoc XRS+ (BIO-RAD) system. Intensity of detected protein bands was quantified by densitometry using Evolution Capture Edge (Vilber Lourmat) or Image Lab (BIO-RAD) software.

2.12. RNA expression analyses throughout mouse and human heart development

To investigate RNA expression of genes throughout mouse and human heart development previously published transcriptome data sets in various organs and mammalian species throughout pre- and postnatal development were used (Cardoso-Moreira et al., 2019) [16]. Raw data (RPKM) for mouse and human hearts were downloaded from the Kaessmann lab website (https://apps.kaessmannlab.org/evodevoapp/) and graphs were generated using Microsoft Excel 2010.

2.13. Statistical analyses

All data were analyzed using SPSS (IBM) or Excel 2010 (Microsoft) software and are presented as mean ± standard error of the mean (SEM). Graphs were generated using Excel or GraphPad Prism 7, the graphical abstract was created with BioRender.com. Data sets were tested for normal distribution by Shapiro-Wilk test and homogeneity of variances between groups was assessed by Levene's test. If these criteria were met, differences between two groups were evaluated with unpaired, two-sided student's *t*-test and those among multiple groups with one-way analysis of variance (ANOVA) followed by Bonferroni post-hoc test. For multiple groups with unequal variance Games Howell post-hoc test was performed. Differences between multiple groups with non-normal distribution were evaluated with non-parametric Kruskal Wallis one-way analysis of variance followed by pairwise comparison of groups. A probability (*P*) value less than 0.05 was considered statistically significant ($^{*}P < 0.05$, $^{**}P < 0.01$ and $^{***}P < 0.001$). Unless stated otherwise, the sample size n for in vitro data indicates the number of separate cell culture wells from one representative experiment. Key

findings were confirmed by a total of 2–3 independent experiments.

3. Results

3.1. Increased expression of genes involved in redox homeostasis in postnatal compared to prenatal mouse and human hearts

Given that postnatal cardiomyocytes switch to an oxidative metabolism which physiologically elevates ROS levels [5–7] we asked whether this is paralleled by an increased capacity to maintain redox homeostasis. We therefore performed Western blot analyses on embryonic (13.5 dpc), fetal (16.5 dpc), neonatal (postnatal day 1, P1) and early adult (8 weeks of age) mouse hearts. Increased mitochondrial mass is represented by markedly higher protein levels of COX IV, a subunit of cytochrome *c* oxidase (complex IV) of the electron transport chain (ETC), in postnatal compared to prenatal hearts (Fig. 1A). At the same time lactate dehydrogenase (LDH), which converts the glycolysis metabolite pyruvate to lactate under anaerobic conditions, is decreased in adult compared to prenatal and newborn hearts (Fig. 1A). Importantly, PRDX proteins form a cysteine sulfonic acid group (Cys-SO3H) upon hyperoxidation which can be used to monitor oxidative stress in Western blot analyses. PRDX-SO3 levels are increased in adult compared to prenatal and newborn hearts thereby clearly confirming increased ROS production (Fig. 1B). Protein levels of NRF2, a transcription factor regulating expression of genes involved in antioxidative defense [13], progressively increase with cardiac maturation (Fig. 1C). Furthermore, protein levels of enzymes involved in ROS detoxification such as SOD1, SOD2 and PRDX3 are significantly increased in adult compared to prenatal or newborn hearts (Fig. 1C) whereas TRX2 is unchanged throughout development (Supplementary Fig. S1). In contrast, the antioxidative enzyme HO-1 shows a reverse expression pattern with high protein levels in the prenatal heart and a decrease after birth (Supplementary Fig. S1). To confirm expression changes of redox genes upon cardiac maturation at the RNA level we used previously published transcriptome data sets in various organs and mammalian species throughout pre- and postnatal development [16]. These analyses confirmed that the expression of multiple antioxidative proteins and enzymes increases after birth and is markedly higher in the adult compared to the prenatal mouse and human heart, including SOD1, SOD2, TXN2 and different PRDX family members (Fig. 1D and E, Supplementary Fig. S2). In conclusion, the switch to an oxidative metabolism and increased mitochondrial respiration in the postnatal heart is paralleled by increased expression of redox proteins which is likely required to cope with high ROS levels in terminally differentiated cardiomyocytes.

3.2. Expression of genes involved in cellular protein homeostasis in the postnatal compared to the prenatal heart

ROS generation along the mitochondrial respiratory chain requires mechanisms to resolve oxidative protein damage. To test whether PQC capacities increase in the postnatal heart we analyzed expression of chaperones as well as components of the HSR and UPR. Interestingly, protein expression of chaperones HSP70 and HSP90 gradually decrease upon progression of murine heart development (Fig. 2A) and HSF1, a key transcription factor of the HSR [12], is reduced in the adult compared to the neonatal heart (Fig. 2A). In contrast, the mitochondrial protease CLPP and the chaperone HSP60 increase in the adult heart, indicating the requirement for high PQC capacities inside mitochondria after the switch to an oxidative metabolism (Fig. 2B). A key step upon activation of the ISR and UPR is phosphorylation of eIF2α which mediates translational inhibition but allows preferential protein synthesis from certain mRNAs, as for example ATF4 [11]. Phosphorylation of eIF2α decreases during cardiac development and is almost undetectable in the adult heart whereas expression of its phosphatase GADD34 does not change (Fig. 2C). Interestingly, we observed an age dependent switch in the molecular weight of eIF2α with a smaller isoform expressed in the embryonic compared to the adult heart (Fig. 2C). ATF4 protein levels peak in the fetal heart but are almost undetectable in adulthood (Fig. 2C). We again evaluated the respective transcriptome data in the mouse and human heart [16]. HSP70 consists of a protein family encoded by different genes, expression of which (e.g. *HSPA4*) is mainly unchanged throughout mouse and human heart development (Supplementary Fig. S3). Similarly, expression of genes encoding HSP90 (e.g. *HSP90AA1*), the ER chaperone BiP/GRP78 (*HSPA5*) or HSP60 (*HSPD1*) either do not show major alterations or tend to decrease with advanced cardiac maturation (Supplementary Fig. S3). UPR genes such as *ATF4*, *DDIT3* (encoding CHOP), *PPP1R15A* (encoding GADD34) or *EIF2A* show variable expression throughout mouse and human heart development but are not considerably induced in the postnatal compared to the prenatal heart (Supplementary Fig. S4). In summary, the postnatal increase in redox proteins is not generally paralleled by similar expression pattern of PQC genes although an induction of mitochondrial PQC proteins is observed in mice after birth.

3.3. Embryonic cardiomyocytes tolerate inhibition of mitochondrial complex III and V but not I

The data presented above suggest significant changes in the capacity to maintain redox homeostasis in the heart upon postnatal maturation. To investigate how immature cardiomyocytes cope with increased ROS generation we treated primary cardiomyocytes isolated from embryonic (12.5–14.5 dpc) mouse hearts with inhibitors of mitochondrial respiration. Cell morphology and density observed by phase-contrast microscopy did not reveal obvious changes after treatment with the ETC complex III inhibitor antimycin A (AMA) or the ATP synthase (i.e. complex V) inhibitor oligomycin (OLI) compared to DMSO treated controls after 24 h (Fig. 3A). In contrast, embryonic cardiomyocytes treated with the ETC complex I inhibitor rotenone (ROT) showed reduced density, cell shrinkage, spherical morphology and detachment (Fig. 3A), which together indicate cell death. Importantly, all three inhibitors reduce ATP levels in H9c2 cells (Supplementary Fig. S5), confirming that the applied concentrations are indeed effective. Given that cell isolations from whole embryonic hearts contain cardiomyocytes and various other cell types (hereafter collectively referred to as non-myocytes) we sought to more specifically monitor the fate of cardiomyocytes upon AMA and OLI treatment. We identified immunofluorescence staining for the cardiac transcription factor Nkx2.5 as reliable marker to differentiate cardiomyocyte from non-myocyte nuclei (Supplementary Figure S6 and Fig. 3B). After 24 h DMSO treatment ~70% of nuclei were Nkx2.5 positive and this proportion is not changed by AMA or OLI (Fig. 3C). This suggests no major impairment of embryonic cardiomyocyte versus non-myocyte growth and survival upon mitochondrial complex III and V inhibition. To further confirm the latter we assessed expression of the cell cycle marker Ki67 after 24 h of OLI or AMA treatment (Fig. 3B). Interestingly, both AMA and OLI reduced cell cycle activity in non-myocytes, whereas cardiomyocytes were only affected by OLI but not AMA (Fig. 3D). Similar results were obtained when using Ki67 in combination with sarcomeric α-actinin as cardiomyocyte marker (Supplementary Figs. S7A and B). Importantly, these results also revealed that ROT completely abolishes cell cycle activity in embryonic cardiomyocytes and has a much stronger effect in non-myocytes compared to AMA and OLI (Supplementary Fig. S7B). To evaluate programmed cell death (apoptosis) we performed immunostaining for cleaved caspase-3 (Supplementary Fig. S7A). Apoptosis was clearly induced in embryonic cardiomyocytes by ROT whereas AMA and OLI only had moderate effects (Supplementary Fig. S7C). In contrast, none of the inhibitors significantly increased apoptosis in non-myocytes (Supplementary Fig. S7C). As a consequence of increased cardiomyocyte death their contribution to the cell composition is reduced after 24 h ROT treatment (Supplementary Fig. S7D). Finally, we measured cardiomyocyte area which revealed that ROT significantly reduced cell size

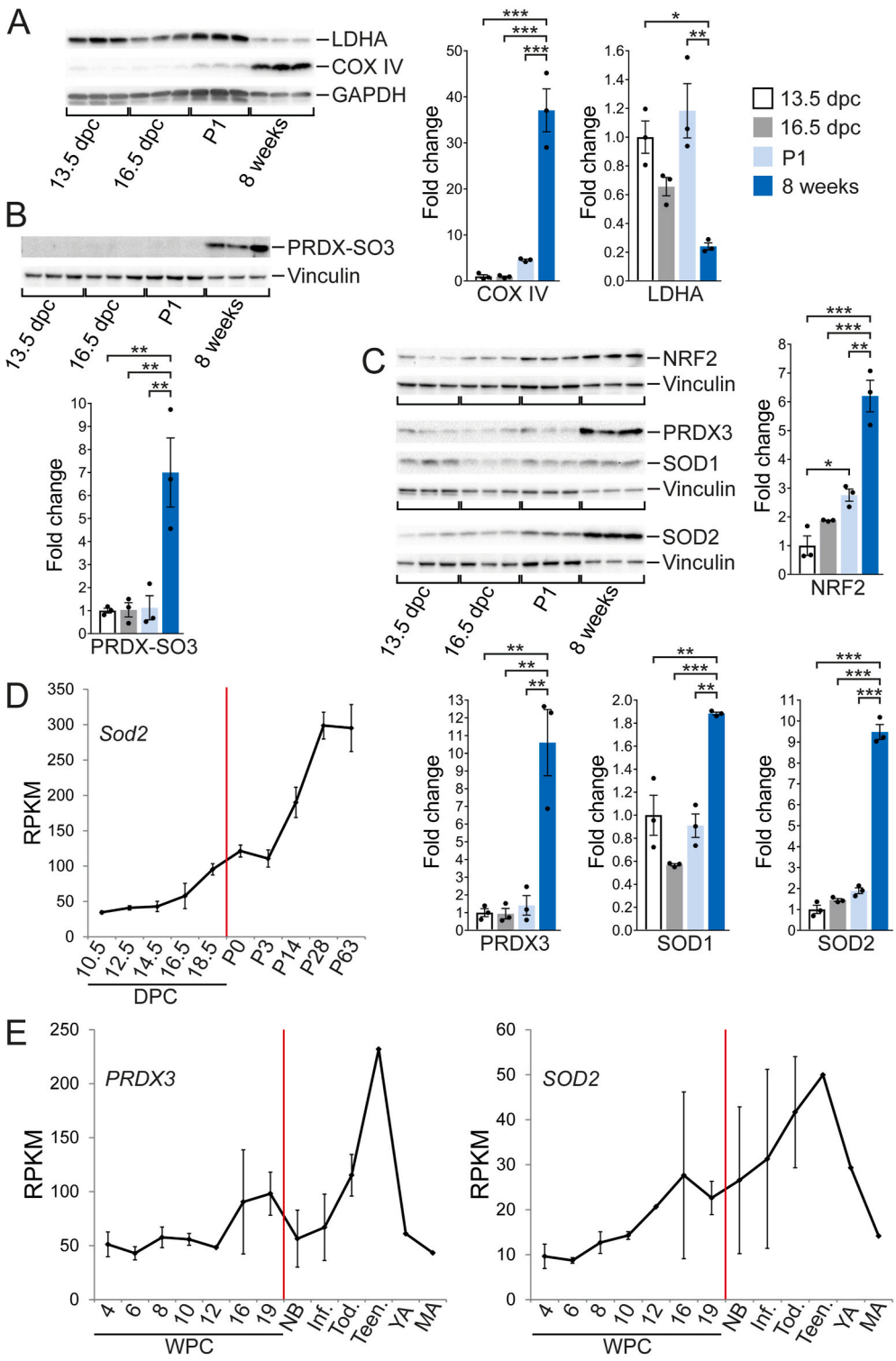

Fig. 1. Expression of genes and proteins involved in redox homeostasis in the pre- and postnatal heart. (A) Western blot analyses showing protein expression of LDHA (lactate dehydrogenase A) and the mitochondrial complex IV subunit COX IV in embryonic (13.5 dpc), fetal (16.5 dpc), neonatal (P1) and adult (8 weeks of age) mouse hearts. (B) Western blot analyses in pre- and postnatal mouse hearts detecting sulfonic acid group (SO3) formation in PRDX (peroxiredoxin) proteins indicating hyperoxidation. (C) Western blot analyses showing protein expression of genes involved in redox homeostasis in pre- and postnatal mouse hearts, including the transcription factor NRF2 (nuclear factor erythroid 2–related factor 2), PRDX3 (peroxiredoxin 3) and the enzymes SOD1 and 2 (superoxide dismutase 1 and 2). (D) RNA expression of *Sod2* at various stages of pre- and postnatal heart development in mice. (E) RNA expression of *PRDX3* and *SOD2* at various stages of pre- and postnatal heart development in humans (data in (D) and (E) derived from Ref. [16], red lines separate pre- and postnatal development, DPC = days post conception, WPC = weeks post conception, P = postnatal day, NB = newborn, Inf. = infant, Tod. = toddler, Teen. = teenager, YA = young adult, MA = mid age). n = 3 mice per group in (A)–(C); $*P < 0.05$, $**P < 0.01$, $***P < 0.001$.

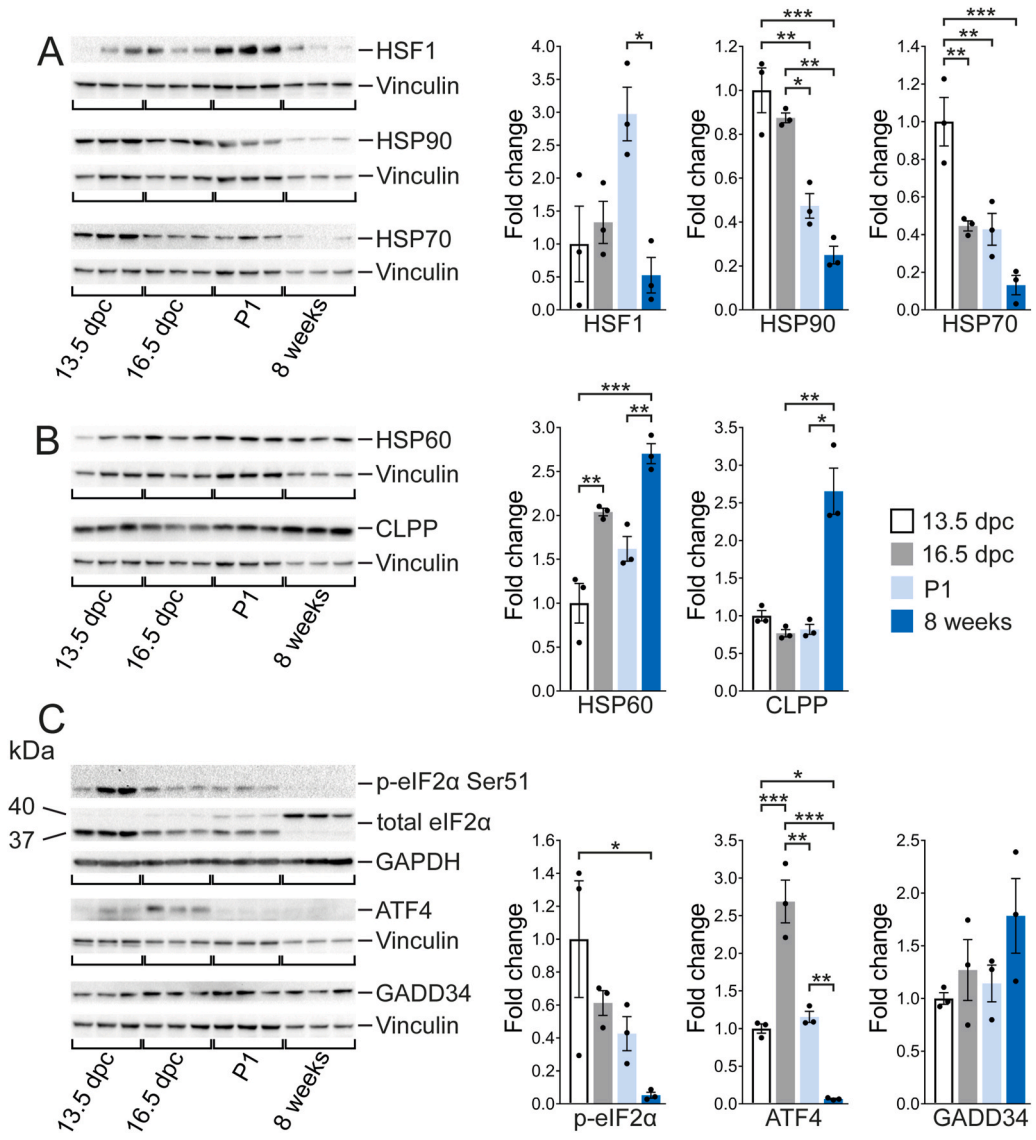

Fig. 2. Expression of proteins involved in cellular protein homeostasis in the pre- and postnatal mouse heart. (A) Western blot analyses of the heat shock response showing protein expression of the transcription factor HSF1 (heat shock factor 1) and the chaperones HSP70 and HSP90 (heat shock protein 70 and 90) in embryonic (13.5 dpc), fetal (16.5 dpc), neonatal (P1) and adult (8 weeks of age) mouse hearts. (B) Western blot analyses of the mitochondrial unfolded protein response showing protein expression of the mitochondrial chaperone HSP60 (heat shock protein 60) and the protease CLPP (caseinolytic mitochondrial matrix peptidase proteolytic subunit) in pre- and postnatal mouse hearts. (C) Western blot analyses of the integrated stress response showing phosphorylation of eIF2α (eukaryotic translation initiation factor 2A) as well as expression of the transcription factor ATF4 (activating transcription factor 4) and the eIF2α phosphatase subunit GADD34 (protein phosphatase 1, regulatory subunit 15 A) in the pre- and postnatal mouse heart. Note the molecular weight switch of total eIF2α with advanced heart maturation. n = 3 mice per group in (A)–(C); $^{*}P < 0.05$, $^{**}P < 0.01$, $^{***}P < 0.001$.

whereas AMA and OLI only had moderate effects (Fig. 3E). In summary, inhibition of mitochondrial complex I induces cell death in embryonic cardiomyocytes but inhibition of complex III and V is well tolerated. Whereas complex V inhibition decreases cell cycle activity complex III inhibition has no detectable effect on growth and survival of embryonic cardiomyocytes.

3.4. Antimycin A induces oxidative stress and alters the mitochondrial network in embryonic cardiomyocytes

The surprising tolerance of embryonic cardiomyocytes towards mitochondrial complex III inhibition raises the question whether AMA is indeed effective under the applied culture conditions. We therefore detected ROS generated within mitochondria using the red fluorescence probe MitoSOX in living cells. This revealed clearly increased fluorescence intensity in AMA compared to DMSO treated embryonic cardiomyocytes after 24 h (Fig. 4A). In addition, detection of hyperoxidized PRDX-SO3 in Western blot analyses showed a marked induction by AMA compared to DMSO (Fig. 4B). To evaluate the intracellular mitochondrial network, we performed immunofluorescence staining for proteins localized within mitochondria, such as SOD2 and HSP60. Both showed markedly different staining pattern in AMA compared to DMSO treated embryonic cardiomyocytes. Whereas SOD2 and HSP60 staining show a structured network predominantly localized in the perinuclear region of DMSO treated cells it is more diffuse and disseminated in the cell periphery upon AMA treatment (Fig. 4C and Supplementary Fig. S8). The latter could indicate increased mitochondrial fission resulting in smaller mitochondria with altered intracellular distribution.

Mitochondrial dysfunction could impair contractility in embryonic cardiomyocytes by altering sarcomere structure. Immunofluorescence staining for sarcomeric α-actinin did not show major differences in sarcomere organization and alignment in AMA compared to DMSO

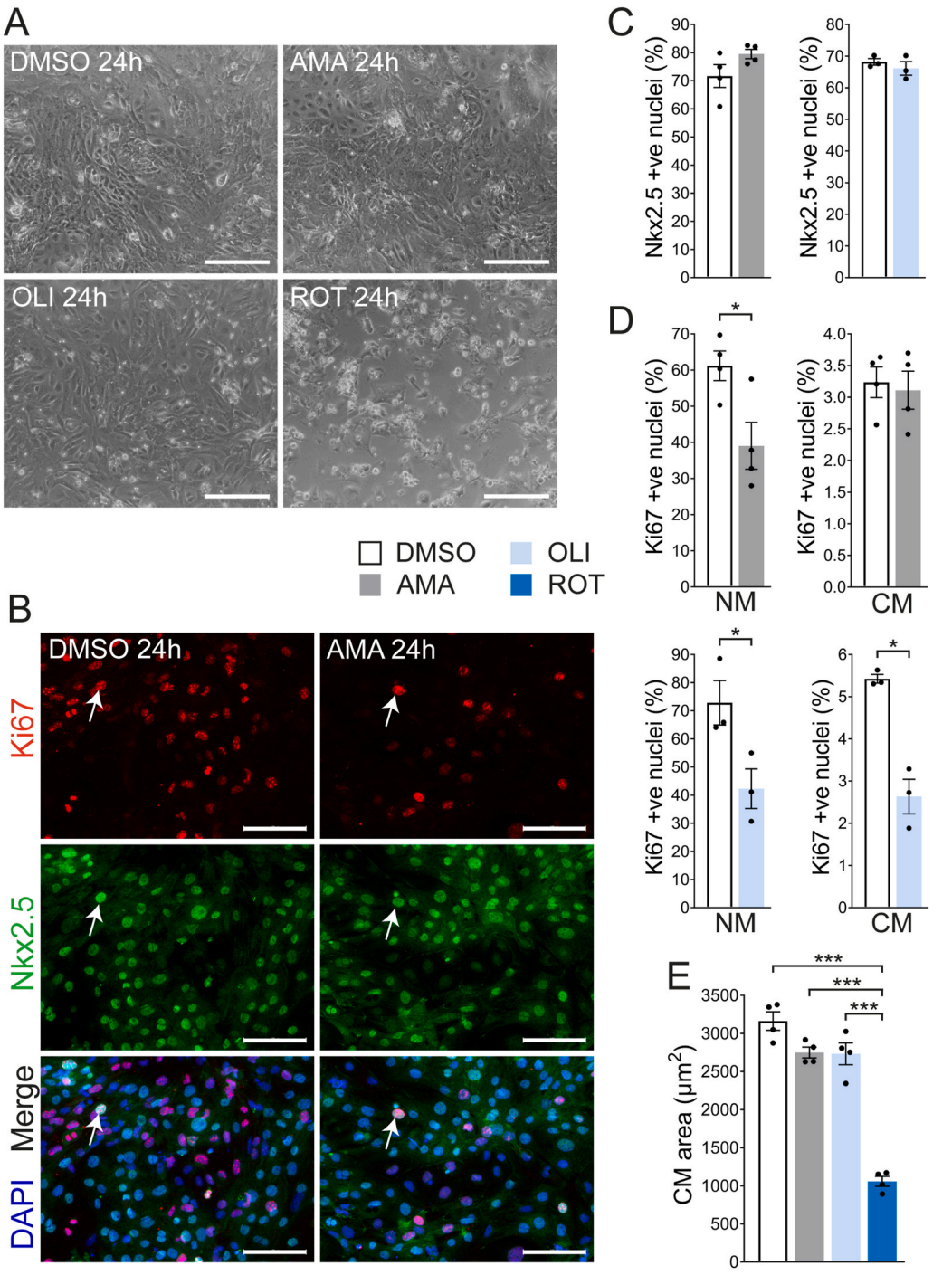

Fig. 3. Morphology and cell cycle activity of embryonic cardiomyocytes treated with inhibitors of mitochondrial respiration. Embryonic cardiomyocytes were treated with DMSO, AMA (50 µM), OLI (5 µM) and ROT (10 µM) for 24 h. (A) Phase-contrast microscopy images (scale bar = 200 µm). (B) Immunofluorescence staining detecting the cell cycle marker Ki67 (in red) and the cardiomyocyte transcription factor Nkx2.5 (in green). Nuclei were stained in blue using DAPI. Arrows indicate examples of Ki67/Nkx2.5 double positive nuclei (scale bar = 100 µm). (C) Contribution of Nkx2.5-positive nuclei to the total number of nuclei as determined by immunofluorescence shown in (B). (D) Cell cycle activity was quantified based on Ki67 immunofluorescence staining in Nkx2.5-negative non-myocyte nuclei (NM) and Nkx2.5 positive cardiomyocyte nuclei (CM). (E) Embryonic cardiomyocytes were treated with DMSO, AMA, OLI and ROT for 24 h (n = 4 wells per treatment) and the cell area was measured based on α-actinin immunofluorescence staining (see Supplementary Fig. S7A). n = 4 wells per treatment for DMSO/AMA and n = 3 for DMSO/OLI in (B) and (D); $^{*}P < 0.05$, $^{***}P < 0.001$.

treated embryonic cardiomyocytes after 24 h (Fig. 4D). We furthermore performed functional evaluations based on phase-contrast microscopy by superimposing a grid over short video frames of embryonic cardiomyocytes and counting squares with visible contractions. Consistent with unaltered sarcomere structure, these results revealed no difference between treatments (Fig. 4E). In conclusion, AMA induces oxidative stress and alters the intracellular mitochondrial network but does not seem to impair contractility in embryonic cardiomyocytes.

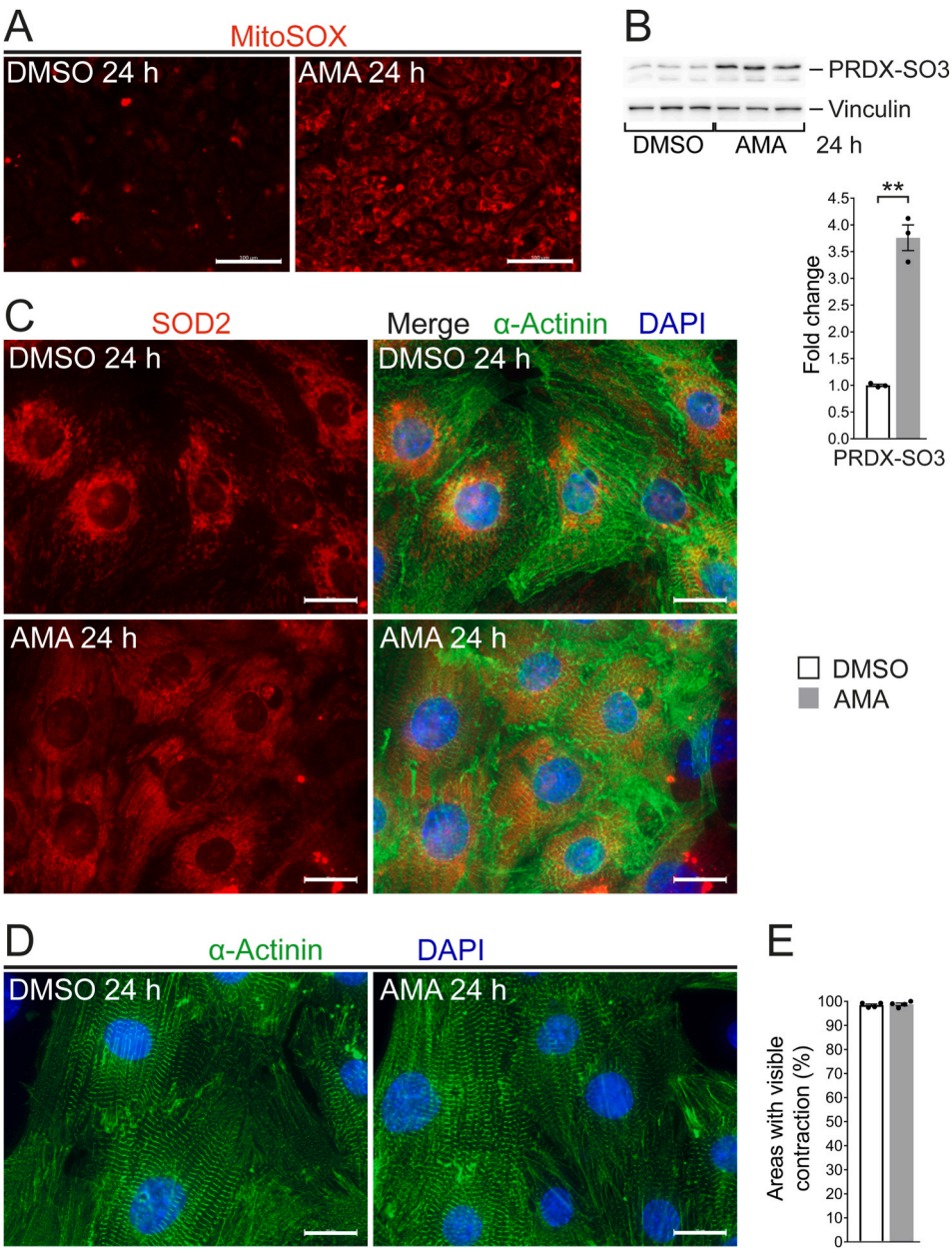

Fig. 4. Oxidative stress, morphology and function in embryonic cardiomyocytes upon mitochondrial complex III inhibition. Embryonic cardiomyocytes were treated with DMSO or AMA (50 μM) for 24 h. (A) Fluorescence microscopy images detecting MitoSOX, a red fluorescent probe for reactive oxygen species generated inside mitochondria (scale bar = 100 μm). (B) Western blot analyses detecting sulfonic acid group (SO3) formation in PRDX (peroxiredoxin) proteins indicating hyperoxidation (n = 3 wells per treatment, $^{**}P < 0.01$). (C) Immunofluorescence staining detecting the mitochondrial ROS detoxifying enzyme SOD2 (in red) and the cardiomyocyte specific sarcomere associated protein α-actinin (in green). Nuclei were stained in blue using DAPI (scale bar = 100 μm). (D) Immunofluorescence staining for α-actinin (in green) showing sarcomere structure and organization at higher magnification (scale bar = 20 μm). (E) Contractility was assessed in phase-contrast microscopy movies with a superimposed grid. Areas with contracting cells were quantified and related to the total number of areas scored (n = 8 wells per treatment).

3.5. Antimycin A activates the integrated stress response and oxidative defense in embryonic cardiomyocytes

To gain molecular insights into the tolerance of embryonic cardiomyocytes towards mitochondrial complex III inhibition we investigated various cellular stress pathways. We have previously shown in mice [17] and cardiac cell lines [18] that immature cardiomyocytes activate the ISR upon complex III inhibition. Similarly, AMA treatment in primary embryonic cardiomyocytes for 24 h increases phosphorylation of eIF2α and protein expression of the ISR transcription factors ATF4 and CHOP (Fig. 5A). Immunofluorescence analyses confirmed ATF4 induction and a predominantly nuclear localization in AMA treated cardiomyocytes as well as in non-myocytes (Fig. 5B).

ATF5 has emerged as key transcription factor mediating the response to mitochondrial stress and regulating the mitochondrial UPR (UPR^{mt}) in mammalian cells [19]. ATF5 tends to be induced in AMA treated embryonic cardiomyocytes (Fig. 5A) and immunofluorescence analyses confirmed increased nuclear localization (Supplementary Fig. S9). However, various components of the UPR^{mt} including YME1L1, PMPCB, ClpP and HSP60 [20] are not induced by AMA on the protein level (Fig. 5C). Mitochondrial dysfunction induces a stress response in the endoplasmic reticulum due to crosstalk between these organelles [21]. Indeed, the ER chaperone GRP78 (also known as BiP), which can indicate ER stress, is strongly induced in AMA treated embryonic

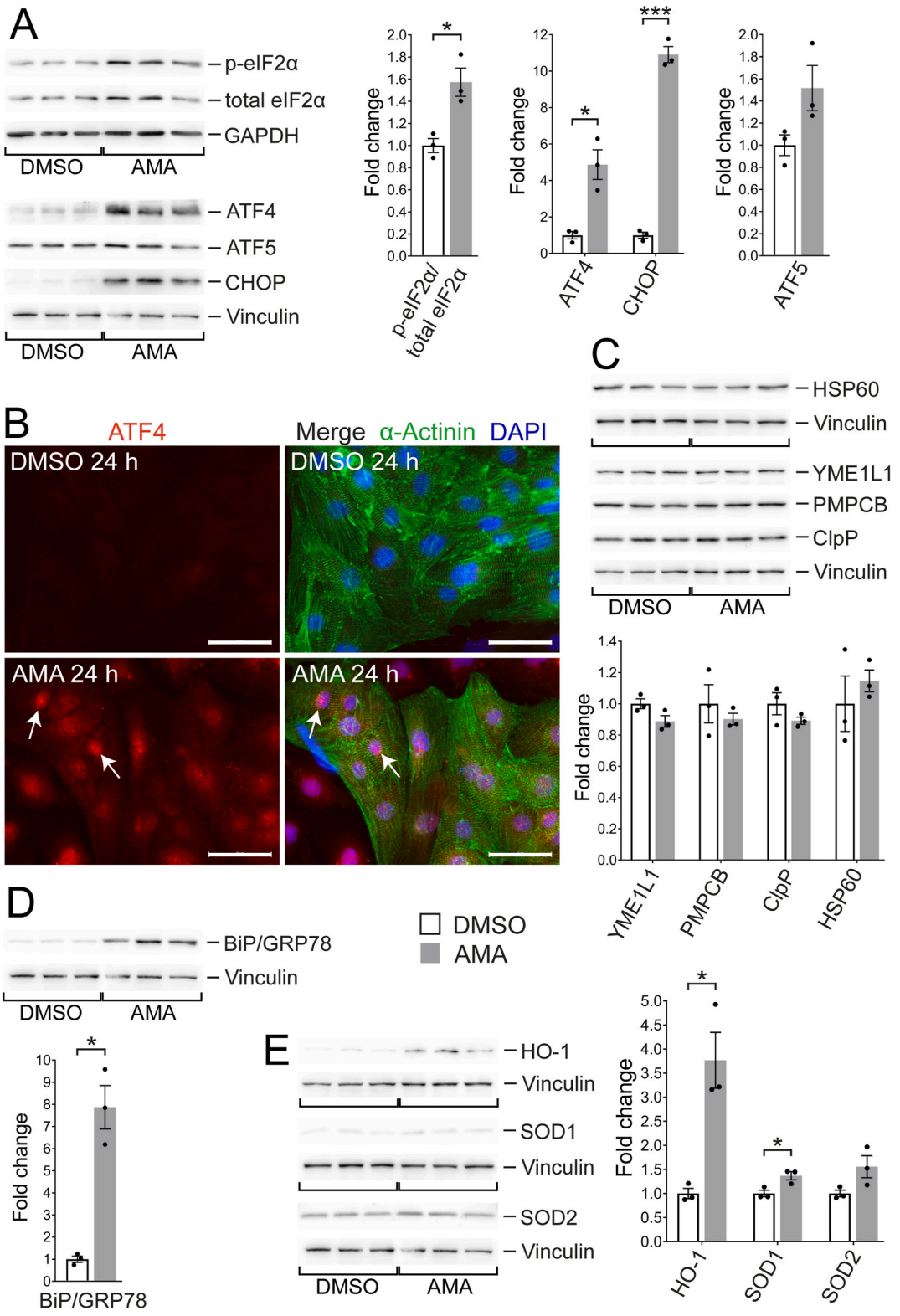

Fig. 5. Stress response in embryonic cardiomyocytes upon mitochondrial complex III inhibition. Embryonic cardiomyocytes were treated with DMSO or AMA (50 μM) for 24 h. (A) Western blot analyses of the integrated stress response (ISR) showing phosphorylation of eIF2α as well as expression of the transcription factors ATF4, CHOP and ATF5. (B) Immunofluorescence staining detecting the ISR transcription factor ATF4 (in red) and the cardiomyocyte specific sarcomere associated protein α-actinin (in green). Nuclei were stained in blue using DAPI (scale bar = 50 μm). Arrows indicate accumulation of ATF4 in cardiomyocyte nuclei. (C) Western blot analyses of the mitochondrial unfolded protein response showing protein expression of the mitochondrial chaperone HSP60 and the proteases/peptidases YME1L1, PMPCB and CLPP. (D) Western blot analyses of ER stress showing protein expression of the ER chaperone BiP (also known as GRP78). (E) Western blot analyses showing protein expression of the antioxidative and ROS detoxifying enzymes HO-1, SOD1 and SOD2. n = 3 wells per treatment in (A) and (C)–(E); $^{*}P < 0.05$, $^{***}P < 0.001$.

cardiomyocytes (Fig. 5D).

We have previously shown in H9c2 cells that AMA induces expression of the HSR transcription factor HSF1 [18], which was not observed in embryonic cardiomyocytes, however (Supplementary Fig. S10A). Moreover, AMA increases phosphorylation of the stress sensitive p38 MAP-kinase in H9c2 cells [18], which is not evident in embryonic cardiomyocytes (Supplementary Fig. S10B). Finally, mitochondrial stress induced by complex III inhibition leads to induction of proteins involved in ROS detoxification in immature cardiac cells both in vivo and in vitro [17,18]. Consistently, AMA increases protein expression of the anti-oxidative proteins SOD1, SOD2 and HO-1 in embryonic cardiomyocytes (Fig. 5E). In summary, mitochondrial complex III inhibition activates the ISR (but not the UPR^{mt}) and oxidative defense in embryonic cardiomyocytes.

3.6. Adult cardiomyocytes rapidly disintegrate upon mitochondrial complex III inhibition

To test how adult cardiomyocytes cope with mitochondrial complex III inhibition they were isolated from 3 to 6 months old murine hearts and treated with AMA. A concentration of 50 μM AMA, which was well tolerated by embryonic cardiomyocytes for up to 24 h, led to rapid

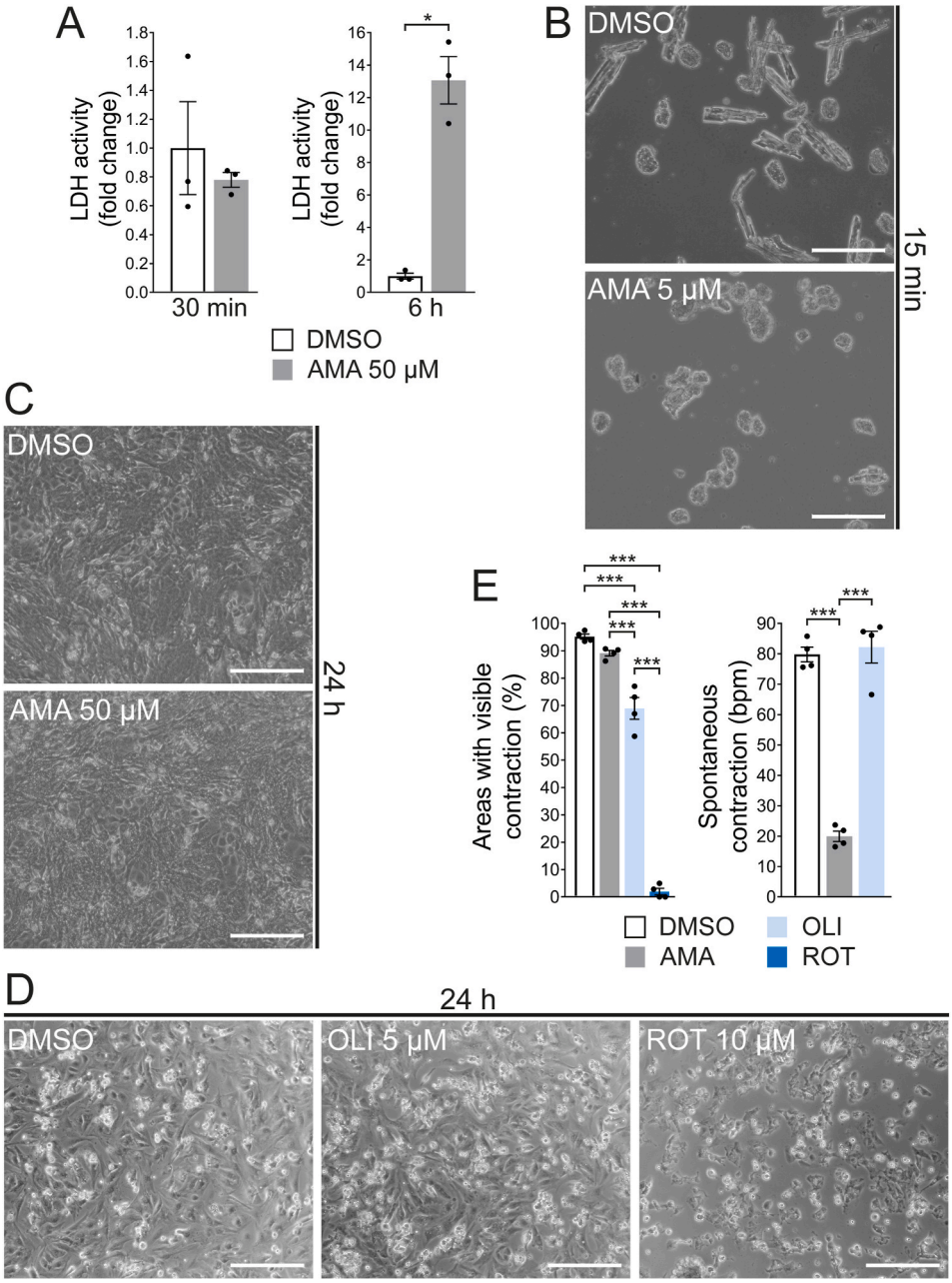

Fig. 6. Survival and morphology of adult and neonatal cardiomyocytes upon mitochondrial dysfunction. (A) LDH activity was measured in the culture medium of adult cardiomyocytes treated with DMSO or AMA (50 μM) for 30 min or 6 h (n = 3 wells per treatment, $^{*}P < 0.05$). (B) Phase-contrast microscopy images of adult cardiomyocytes treated with DMSO or AMA (5 μM) for 15 min. (C) Phase-contrast microscopy images of neonatal cardiomyocytes treated with DMSO or AMA (50 μM) for 24 h. (D) Phase-contrast microscopy images of neonatal cardiomyocytes treated with DMSO, OLI (5 μM) and ROT (10 μM) for 24 h (scale bar = 200 μm in (B)–(D)). (E) Neonatal cardiomyocytes were treated with DMSO, AMA (50 μM), OLI (5 μM) or ROT (10 μM) for 24 h and contractility was assessed in phase-contrast microscopy with a superimposed grid. Areas with contracting cells were quantified and related to the total number of areas scored and the frequency of spontaneous contraction (bpm = beats per minute) was determined (n = 4 wells per treatment, $^{***}P < 0.001$).

changes in cell morphology. Whereas the majority of DMSO treated adult cardiomyocytes was rod shaped and attached to the culture flask for several hours, AMA treated cells showed a rounded and spherical shape after 30 min (Supplementary Fig. S11A). In addition, the majority of cells had detached and was floating in the medium. 6 h after the onset of AMA treatment increased LDH activity in the culture medium compared to DMSO treated cells indicated cellular disintegration, which was not yet observed after 30 min despite detachment and altered cell shape (Fig. 6A). The rapid changes in cell morphology were similarly observed with 10 μM and 5 μM AMA, a concentration 10 times lower compared to that tolerated by embryonic cardiomyocytes. Adult cardiomyocytes started to round up and detach as soon as 5 min after the onset of treatment (Supplementary Fig. S11B) and after 15 min rod shaped cells were no longer observed (Fig. 6B). Thus, adult cardiomyocytes are highly susceptible to mitochondrial complex III inhibition and undergo rapid cellular disintegration.

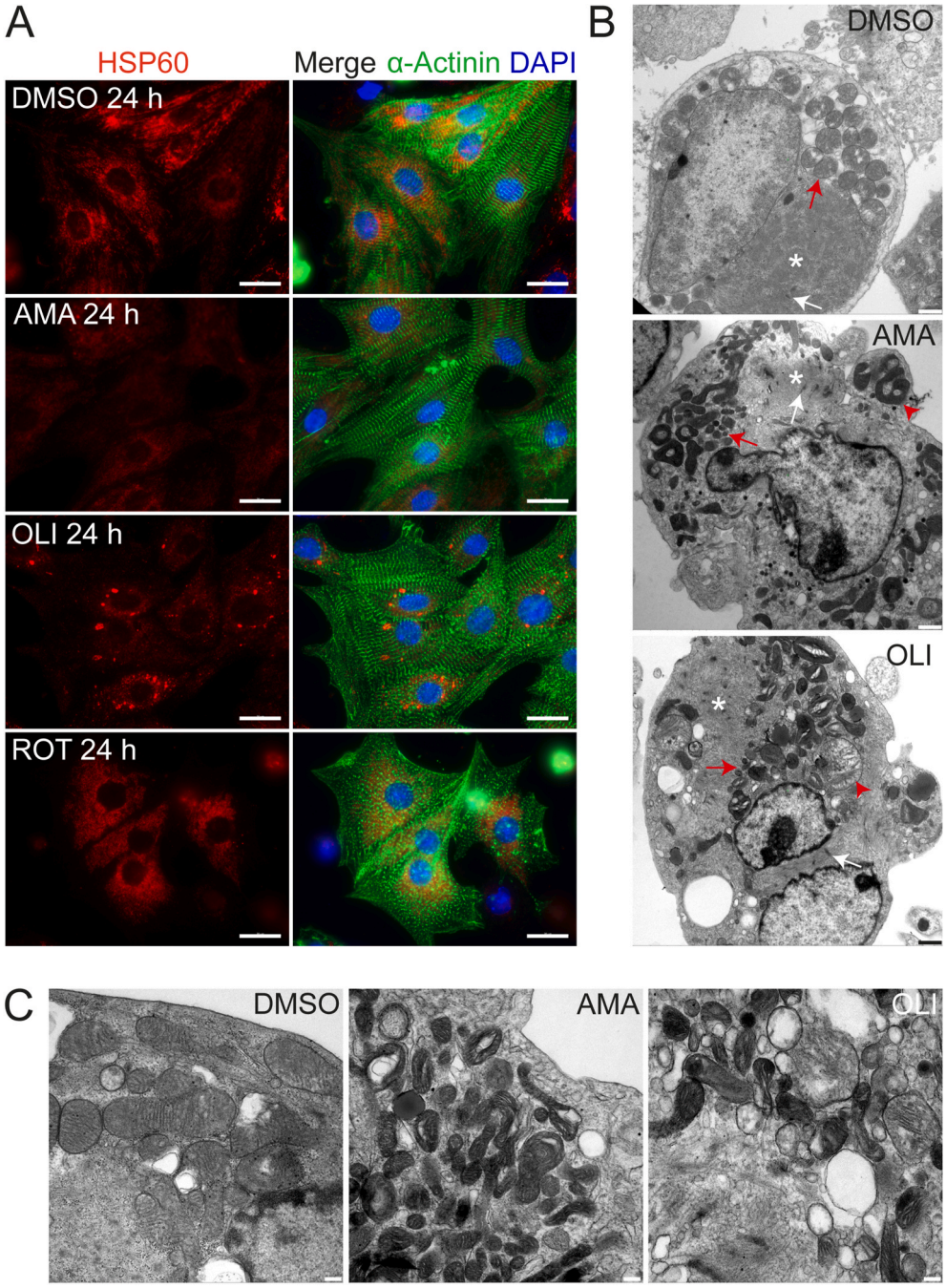

Fig. 7. Sarcomere organization and mitochondrial ultrastructure in neonatal cardiomyocytes treated with inhibitors of mitochondrial respiration. (A) Immunofluorescence staining of neonatal cardiomyocytes treated with DMSO, AMA (50 μM), OLI (5 μM) and ROT (10 μM) for 24 h detecting the mitochondrial chaperone HSP60 (in red) and the cardiomyocyte specific sarcomere associated protein α-actinin (in green). Nuclei were stained in blue using DAPI (scale bar = 20 μm). (B) Transmission electron microscopy (TEM) images of neonatal cardiomyocytes treated with DMSO, AMA (50 μM) and OLI (5 μM) for 24 h. Cardiomyocytes were identified based on the presence of myofibrils (see white asterisks) and sarcomere structures such as z-discs (see white arrows). Mitochondria are indicated by red arrows. Red arrowheads point to extremely misshaped (AMA) or enlarged (OLI) mitochondria (scale bar = 1000 nm). (C) High power TEM images of neonatal cardiomyocytes treated as described above to show mitochondrial morphology and ultrastructure (scale bar = 250 nm).

3.7. Neonatal cardiomyocytes behave similar to embryonic cardiomyocytes upon inhibition of mitochondrial respiration

If resistance towards mitochondrial dysfunction is lost during cardiomyocyte terminal differentiation, it might still be preserved in the perinatal phase. Therefore, neonatal mouse cardiomyocytes were isolated on postnatal day 1 (P1) and treated with AMA (50 μM), OLI (5 μM) and ROT (10 μM). Interestingly, no major differences in cell density and no signs of excessive cell death (i.e. detached or floating cells) were observed in AMA and OLI compared to DMSO treated cells after 24 h (Fig. 6C and D). In contrast, ROT treatment results in severely disturbed cell morphology (i.e. shrinkage, globular shape and fragmentation), detachment and reduced cell density (Fig. 6D). Immunofluorescence staining for Ki67 and α-actinin revealed that all three inhibitors reduced cell cycle activity in non-myocytes with ROT having the most severe effect (Supplementary Figs. S12A and B), a result similar to cells isolated from the embryonic heart described above. In contrast to embryonic cardiomyocytes, all three inhibitors including AMA reduced cell cycle activity and size in neonatal cardiomyocytes (Supplementary Figs. S12B and C).

Functional analyses by counting areas with visible contractions in phase-contrast microscopy revealed that neonatal cardiomyocytes treated with AMA showed contractile areas similar to DMSO after 24 h but contractility was reduce by OLI and almost absent after ROT treatment (Fig. 6E). The frequency of spontaneous contractions, however, was unaffected by OLI but clearly reduced by AMA (Fig. 6E). Thus, whereas ROT abolishes contractility in neonatal cardiomyocytes and causes cellular disintegration, AMA and OLI are largely tolerated but have moderate but differential effects on contractile function.

3.8. Neonatal cardiomyocytes exhibit changes in mitochondrial ultrastructure when treated with mitochondrial inhibitors

Consistent with the contractility results described above, immunofluorescence staining for α-actinin revealed largely normal sarcomere organization and alignment in AMA and OLI compared to DMSO treated neonatal cardiomyocytes. In contrast, ROT leads to disassembled and fragmented sarcomeres evident as speckled α-actinin staining (Fig. 7A). To assess organization of the intracellular mitochondrial network immunofluorescence staining for HSP60 was performed. This revealed a predominantly perinuclear localization of mitochondria in DMSO treated neonatal cardiomyocytes with numerous extensions in the cell periphery (Fig. 7A). In contrast, HSP60 staining is much weaker and diffusely distributed within AMA treated cardiomyocytes whereas a stronger but similarly diffuse staining pattern was observed upon ROT treatment (Fig. 7A). Interestingly, HSP60 staining in OLI treated cardiomyocytes is characterized by bright and punctuated structures in the perinuclear region (Fig. 7A). Thus, the inhibitors of mitochondrial respiration have different consequences for the organization of the mitochondrial network within neonatal cardiomyocytes.

To further evaluate the latter we performed transmission electron microscopy (TEM) in cultured cells isolated from the neonatal mouse heart and treated with AMA or OLI for 24 h. Cardiomyocytes could readily be identified in TEM images based on the presence of myofibrils and sarcomere structures (Fig. 7B). DMSO treated cardiomyocytes contained relatively large and uniformly round mitochondria with a loose but well organized cristae structure. In contrast, AMA and OLI treated cardiomyocytes showed remarkable mitochondrial polymorphisms with a large number of small and round mitochondria but also elongated or totally misshaped mitochondria presenting as ring-like structure with apparent inclusions (Fig. 7B and C). In addition, OLI treated cardiomyocytes occasionally contain some extremely enlarged mitochondria which could represent the punctuated structures seen in HSP60 immunofluorescence staining. In summary, mitochondrial dysfunction in neonatal cardiomyocytes leads to alterations of the mitochondrial network und ultrastructure.

3.9. Antimycin A treatment in adult cardiomyocytes leads to inactivation of the integrated stress response

Adult cardiomyocytes rapidly undergo cell death upon AMA treatment with LDH release in the culture medium detected after 6 h (Fig. 6A). Consequently, Western blot experiments after 6 h and 24 h AMA treatment (50 μM) revealed loss of the majority of proteins, including cytoplasmic (GAPDH, HSP70 and HSP90) as well as structural and cytoskeletal (vinculin and tubulin) proteins indicative of cellular disintegration (Supplementary Fig. S13). Interestingly, proteins localized within mitochondria (HSP60 and SOD2) or the ER (GRP78/BiP) were still detectable, suggesting that these organelles are somewhat preserved (Supplementary Fig. S13). To gain insights into the stress response of adult cardiomyocytes we performed Western blot analyses after 15 and 30 min AMA treatment, a period after which LDH release was not yet detected (Fig. 6A). Importantly, hyperoxidation of PRDX was observed at both time points confirming a rapid increase in ROS generation (Fig. 8A). Expression of proteins involved in antioxidative defense was not altered in adult cardiomyocytes after 15 or 30 min AMA compared to DMSO treatment (Supplementary Fig. S14A), similar to chaperones HSP60, HSP70 and HSP90 (Supplementary Fig. S14B). When investigating the ISR we found reduced phosphorylation of eIF2α and reduced ATF4 and CHOP expression after AMA compared to DMSO treatment (Fig. 8B). Thus, a rapid onset of oxidative stress by mitochondrial complex III inhibition is accompanied by inhibition of the ISR in adult cardiomyocytes.

3.10. Embryonic and adult cardiomyocytes show a different stress response after mitochondrial complex III inhibition

Rapid disintegration of adult cardiomyocytes upon AMA treatment precludes meaningful comparisons with embryonic cardiomyocytes regarding molecular stress response mechanisms. We therefore titrated an AMA concentration that is tolerated by adult cardiomyocytes for a longer period and found that 1 μM for 2 h results in moderate morphological changes with the majority of cells still being rod shaped (Supplementary Fig. S15). Thus, we directly compared stress response pathways in embryonic and adult cardiomyocytes treated with 50 μM or 1 μM AMA, respectively, for 2 h. Hyperoxidation of PRDX was not observed in both groups (Supplementary Fig. S16A) suggesting that oxidative stress is still kept in check. Importantly, 50 μM AMA results in PRDX-SO3 formation after 15 min in adult cardiomyocytes (Fig. 8A) whereas no changes are observed in embryonic cardiomyocytes for up to 2 h. These data indicate fundamental differences in the dynamics of ROS generation upon mitochondrial dysfunction in embryonic versus adult cardiomyocytes.

Western blot analyses showed increased levels of mitochondrial (COX IV) and antioxidative (PRDX3 and SOD2) proteins in adult versus embryonic cardiomyocytes (Supplementary Fig. S16A), similar to in vivo data during heart development described above (Fig. 1A and C). However, PRDX3 and SOD2 were not induced by AMA compared to DMSO in either cell type after 2 h (Supplementary Fig. S16A). The HSR transcription factor HSF1 showed lower protein expression in adult versus embryonic cardiomyocytes (Fig. 8C) as shown in vivo (Fig. 2A). Whereas HSF1 is not affected in AMA treated embryonic cardiomyocytes it is reduced by AMA in adult cardiomyocytes (Fig. 8C). The ER chaperone BiP/GRP78 also showed lower protein levels in adult versus embryonic cardiomyocytes but is not affected by AMA in either cell type (Supplementary Fig. S16B). Thus, ER stress observed in embryonic cardiomyocytes after 24 h (Fig. 5D) appears to be a late but not an immediate response to mitochondrial complex III inhibition. When investigating the UPR^{mt} we found no changes in ATF5, HSP60 or YME1L1 protein expression in AMA versus DMSO treated embryonic or adult cardiomyocytes, respectively (Supplementary Fig. S16C). In contrast, phosphorylation of eIF2α was increased by AMA in both cell types (Fig. 8D). Thus, whereas high AMA concentrations associated with

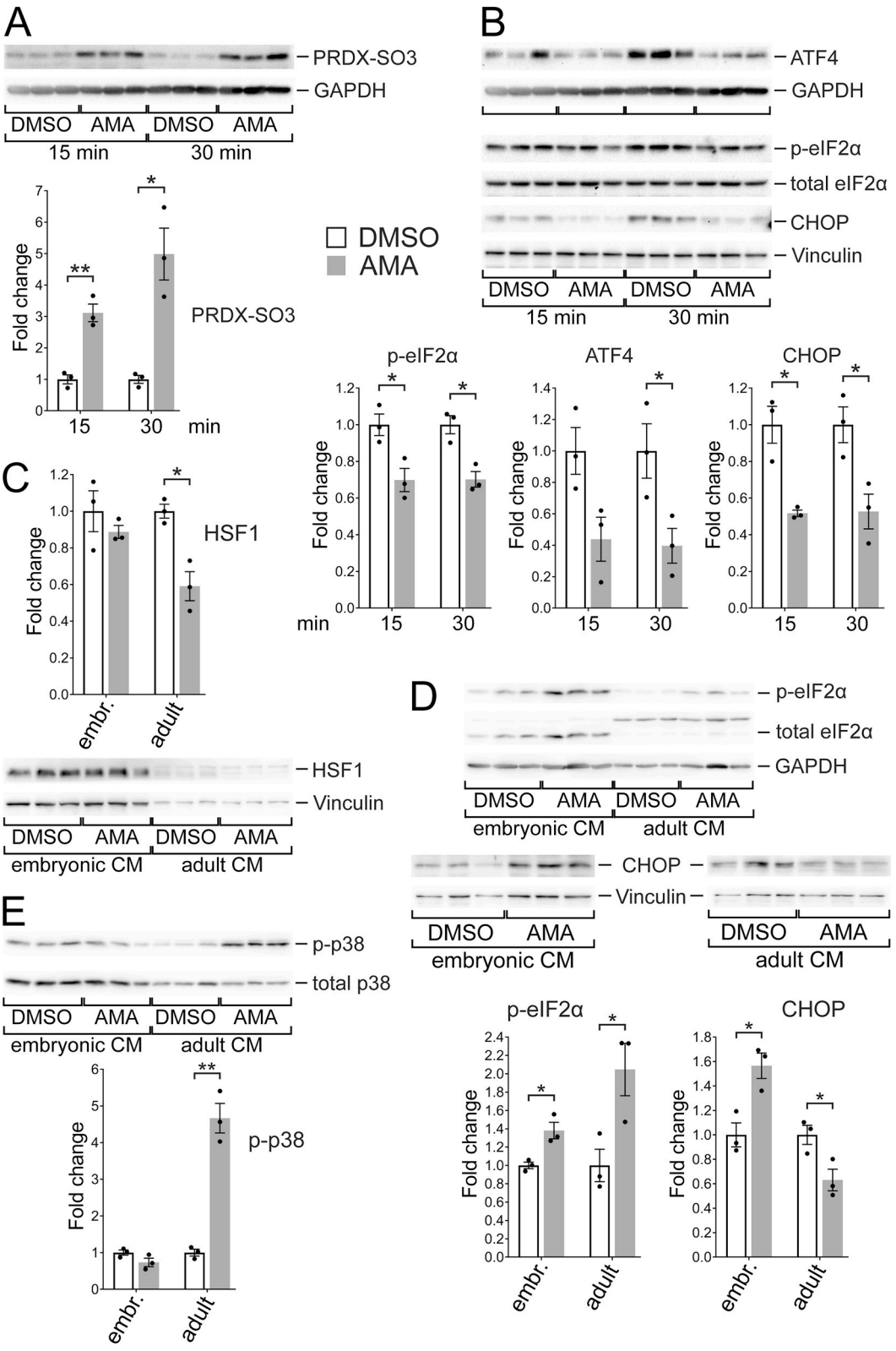

Fig. 8. Stress response in adult compared to embryonic cardiomyocytes upon mitochondrial complex III inhibition. (A) Adult cardiomyocytes were treated with DMSO or AMA (50 μM) for 15 or 30 min. Western blot analyses show sulfonic acid group (SO3) formation in PRDX (peroxiredoxin) proteins indicating hyperoxidation. (B) Western blot analyses of the integrated stress response showing phosphorylation of eIF2α as well as expression of the transcription factors ATF4 and CHOP in adult cardiomyocytes treated as described in (A). (C) Embryonic and adult cardiomyocytes (CM) were treated with DMSO or AMA (50 μM and 1 μM, respectively) for 2 h. Western blot analyses show protein expression of the transcription factor HSF1. (D) Western blot analyses of the integrated stress response showing phosphorylation of eIF2α and expression of the transcription factor CHOP in embryonic and adult cardiomyocytes treated as described in (C). Note the molecular weight switch of total eIF2α in embryonic versus adult cardiomyocytes. (E) Western blot analyses showing phosphorylation of p38 MAP-kinase in embryonic and adult cardiomyocytes treated as described in (C). n = 3 wells per cell type and treatment in all panels; $*P < 0.05$, $**P < 0.01$.

cellular disintegration reduce eIF2α phosphorylation (Fig. 8B), moderate oxidative stress increases the latter in adult cardiomyocytes. Intriguingly, the ISR transcription factor and downstream effector CHOP is increased by AMA in embryonic but reduced in adult cardiomyocytes (Fig. 8D). Thus, regulation of the ISR downstream of eIF2α phosphorylation in response to mitochondrial complex III inhibition seems to differ in embryonic compared to adult cardiomyocytes.

Finally, we have previously shown that stress responsive p38 MAP-kinase is activated by AMA in cardiac cell lines [18]. Interestingly, whereas phosphorylation of p38 was not altered in AMA treated embryonic cardiomyocytes after 2 h, it was strongly induced in adult cardiomyocytes (Fig. 8E). Taken together, in addition to striking differences in survival of embryonic versus adult cardiomyocytes in response to high AMA concentrations, even sub-lethal complex III inhibition results in differential regulation of stress response mechanisms including the ISR, HSF1 and p38 MAP-kinase.

4. Discussion

Cardiomyocyte differentiation throughout pre- and postnatal heart development involves a multitude of critical steps to eventually generate highly specialized cells that allow efficient contraction. Mitochondrial maturation in cardiomyocytes is characterized by an increase in mass after birth accompanied by a switch towards an oxidative metabolism [4–6]. The latter is required for sufficient ATP supply but also comes with increased ROS generation along the mitochondrial ETC [7,8]. Whether cardiomyocyte terminal differentiation therefore includes adaptations of cellular redox and PQC mechanisms to establish stress tolerance in the postnatal heart is incompletely understood. The current study shows that genes and proteins involved in ROS detoxification [13] are increased at the RNA and protein level in the mouse heart after birth. The same trend in RNA expression is observed in humans. In contrast, genes involved in PQC such as chaperones or components of the ISR/UPR [9–12] show only moderate changes in RNA expression in the pre- versus postnatal human and mouse heart. Exceptions are proteins specifically involved in mitochondrial PQC (i.e. HSP60 and CLPP) [19,20] which increase in the postnatal mouse heart. In summary, postnatal cardiomyocyte maturation is paralleled by the induction of genes involved in redox homeostasis and mitochondrial PQC which are likely required to compensate for the consequences of an oxidative metabolism.

Even though the postnatal increase in redox capacities protects adult cardiomyocytes from physiological ROS production, mitochondrial dysfunction boosts ROS levels [2,3,8]. Indeed, our results clearly show that cardiomyocyte differentiation affects susceptibility towards complex III inhibition. Whereas embryonic and neonatal cardiomyocytes largely tolerate AMA treatment for at least 24 h, adult cardiomyocytes undergo disintegration within minutes. These results are in agreement with our previous studies in cardiac cell lines which revealed that immature H9c2 cardiomyoblasts tolerate AMA treatment whereas more differentiated HL-1 cells do not [18]. Furthermore, studies in mouse embryos have shown that cardiomyocytes lacking the mitochondrial electron transport protein cytochrome *c* are not eliminated during heart development and survive until adulthood [17]. An intriguing question is what protects immature cardiomyocytes from mitochondrial complex III inhibition? An obvious explanation might be the primary reliance on a glycolytic metabolism [5,6]. That way electron flux along the respiratory chain is low leading to moderate ROS production even under pathological conditions. In contrast, the high oxidative metabolism of adult cardiomyocytes causes excessive electron leakage upon mitochondrial dysfunction resulting in high ROS levels and oxidative damage [2,3,8]. Alternatively, immature cardiomyocytes might be better equipped to deal with oxidative stress, either by more efficient ROS detoxification or more effective repair of oxidative damage. Finally, energy demands can potentially be met via glycolysis in immature cardiomyocytes subjected to mitochondrial dysfunction. Adult cardiomyocytes, in contrast, heavily rely on ATP generated by oxidative phosphorylation such that ATP depletion has more severe consequences. The latter might affect ATP dependent processes required to maintain basic cellular functions and membrane integrity [1–3]. Given the rapid disintegration of adult cardiomyocytes it appears likely that rupture of the plasma membrane is involved in the induction of cell death. The latter therefore likely represents necrosis rather than programmed cell death which would not be executed within minutes after the onset of mitochondrial dysfunction [22]. Interestingly, under pathological conditions adult cardiomyocytes undergo metabolic reprogramming resulting in altered substrate utilization and reduced fatty acid oxidation [23]. Whether the latter contributes to bypassing mitochondrial respiration thereby preventing excessive ROS production and oxidative damage is incompletely understood.

To uncover differences between embryonic and adult cardiomyocytes subjected to mitochondrial complex III inhibition we characterized various cellular stress response mechanisms previously identified in cardiac cell lines and embryonic mouse hearts [17,18]. A striking observation was an activation of the ISR in embryonic but an inactivation in adult cardiomyocytes in response to AMA. Activation of the ISR has previously been observed in immature H9c2 cardiomyoblasts but it is not required for their survival upon AMA treatment [18]. Similarly, HL-1 cells activate the ISR upon complex III inhibition but pharmacological ISR augmentation does not reduce cell death [18]. In adult cardiomyocytes treated with high AMA concentrations the detrimental changes resulting in rapid cellular disintegration might not allow a coordinated ISR activation. Adult cardiomyocytes treated with low dose AMA show eIF2α phosphorylation but no induction of CHOP. Thus, differential activation and regulation of the ISR might be involved in cell fate of embryonic versus adult cardiomyocytes upon complex III inhibition. Interestingly, the inability to activate or maintain ISR signaling during ER stress contributes to cell death in macrophages [24].

Additional differences include reduced HSF1 protein expression and increased p38 MAP-kinase phosphorylation in AMA treated adult but not embryonic cardiomyocytes. HSF1 can protect cardiomyocytes in the adult heart [25] and its reduction may increase the susceptibility of adult cardiomyocytes to cell death. However, HSF1 is induced in AMA treated H9c2 cells but is not required for their survival [18]. p38 MAP-kinase executes multiple functions in the heart but can promote myocardial injury and cardiomyocyte death under pathological conditions [26,27]. Nevertheless, whether changes in HSF1 and p38 are causatively involved in the rapid disintegration of adult cardiomyocytes upon mitochondrial complex III inhibition or just confounding observations is unclear. In AMA treated H9c2 cells antioxidative defense downstream of the transcription factor NRF2 is required for growth and survival [18]. Induction of enzymes involved in ROS detoxification is also observed in AMA treated embryonic cardiomyocytes whereas the rapid changes in adult cardiomyocytes likely precede activation of the respective proteins. Nevertheless, augmenting NRF2 signaling has been shown to be cardioprotective in the adult heart [28].

Embryonic and neonatal mouse cardiomyocytes show a different outcome depending on which mitochondrial complex is functionally impaired. Whereas inhibition of complex III and V is relatively well tolerated, inhibition of complex I causes severe changes in cell morphology and death, findings that are in agreement with previous results in H9c2 cells [18]. AMA and ROT doses applied in H9c2 cells result in similar ROS levels [18] and all three components cause ATP depletion (this study). A possible explanation for the different outcomes is that complex I releases ROS in the mitochondrial matrix whereas complex III releases ROS in the matrix and the intermembrane space from where it can more easily reach the cytoplasm [29]. That way, compartment overlapping ROS detoxification machineries might be more efficiently accessible upon complex III inhibition thereby attenuating the overall burden of oxidative damage [30]. Complex V itself does not produce ROS but OLI treatment results in hyperpolarization of the inner mitochondrial membrane thereby inducing electron leakage and

ROS production along the ETC [8]. How ROS are distributed within the cell in this scenario is not fully established. Furthermore, inhibition of ATP synthase in cancer cells can result in metabolic reprogramming in favor of glycolysis as well as ROS mediated activation of a pro-survival program involving NFκB signaling and anti-apoptotic BCL-proteins [31]. Whether immature cardiomyocytes harbor a similar plasticity to deal with mitochondrial dysfunction is an intriguing question in future studies.

Even though oxidative stress is harmful for the heart, ROS are also physiological signaling molecules involved in various cardiovascular processes [32]. This seems particularly relevant for immature cardiomyocytes given that cardiomyocyte differentiation from iPS cells in vitro requires ROS [33]. Furthermore, differentiation of embryonic mouse cardiomyocytes is regulated by the mitochondrial permeability transition pore and depends on ROS levels [34]. In contrast, mitochondrial dysfunction and elevated ROS levels impair cardiomyocyte proliferation in the embryonic mouse heart resulting in reduced heart size and intrauterine lethality [35]. Mitochondrial dysfunction in the immediate postnatal period, however, does not affect cardiomyocyte maturation when considering sarcomere organization and cell dimensions even though it impairs calcium handling and contractility [35]. AMA and OLI treatment do not disturb sarcomere structure and organization in embryonic and neonatal cardiomyocytes whereas ROT causes sarcomere disassembly. Oxidative modifications of sarcomere proteins have been reported leading to different degrees of contractile impairment [36]. Interestingly, our results suggest that the type and source of ROS has an impact given that ROS generated from complex I have more severe consequences for sarcomere assembly in immature cardiomyocytes.

Mitochondrial morphology and intracellular localization are differentially affected by the various inhibitors of respiration in cultured embryonic and neonatal cardiomyocytes. Immunofluorescence analyses show that mitochondria normally accumulate in the perinuclear region but AMA and ROT result in a diffuse and disseminated localization throughout the cell. OLI causes yet another pattern characterized by clustered aggregation of mitochondria in the perinuclear region. TEM analyses confirmed marked differences in mitochondrial size, morphology and structure in AMA and OLI treated neonatal cardiomyocytes, mainly characterized by an increased number of small mitochondria compared to controls. Mitochondrial dynamics play a major role in cardiomyocyte stress response and survival under various pathological conditions [37,38]. Mitochondrial fission generally occurs upon stress thereby allowing damaged mitochondria to be more easily accessible for mitophagy while at the same time facilitating biogenesis from the remaining intact mitochondria [39]. Our data suggest that all three inhibitors applied primarily cause mitochondrial fragmentation in neonatal cardiomyocytes, whereas ATP synthase inhibition might furthermore result in occasional mitochondrial hyperfusion or swelling, as shown in other studies [40,41].

Limitations of the current study include the in vitro approach which does not resemble the complexity of myocardial tissue and its influence on cardiomyocyte survival, including interaction with other cell types, growth factors, cytokines, metabolites, extracellular matrix components and many more. Given that some of these factors might be protective whereas others are detrimental, cardiomyocyte survival upon mitochondrial dysfunction in vivo might be different. Moreover, we did not identify the molecular mechanisms that protect embryonic cardiomyocytes from mitochondrial complex III inhibition neither did we characterize differences in stress response induced by AMA compared to ROT or OLI treatment. Although we performed the respective experiments in H9c2 cells in a previous study [18], primary cardiomyocytes likely differ in this regard. Along these lines, the onset and dynamics of mitochondrial dysfunction was not characterized in full detail in immature cardiomyocytes treated with different mitochondrial inhibitors. Thus, we cannot definitively claim that stress levels were comparable at any time such that outcomes might be influenced by variable severity of mitochondrial impairment. Finally, throughout this study primary cardiomyocytes were isolated from C57BL/6J mice which harbor an inactivating mutation in the NTT (nicotinamide nucleotide transhydrogenase) gene that affects mitochondrial redox homeostasis [42]. Even though this mutation is generally believed to increase oxidative stress it has been shown to be protective in the heart upon pressure overload [43]. Nevertheless, we cannot formally exclude that abnormal NTT function might have an impact on some of the in vitro results reported here.

In summary, this study shows that cardiomyocyte maturation during pre- and postnatal heart development is accompanied by increased capacities to maintain redox homeostasis and mitochondrial protein quality control. Failure to achieve full potential of the latter after birth, as recently proposed in children with dilated cardiomyopathy (DCM) [44], might contribute to the pathogenesis or progression of pediatric heart disease. Furthermore, immature cardiomyocytes show remarkable tolerance towards mitochondrial dysfunction induced by inhibition of complex III and V and fetal human cardiomyocytes have been proposed to largely tolerate ischemia and reperfusion [45]. Such plasticity of embryonic and fetal cardiomyocytes might be essential to outlast periods of unfavorable or pathological intrauterine conditions to sustain heart growth and prevent structural defects or perinatal heart disease. In this regard, uncompensated mitochondrial oxidative stress has been proposed to be involved in the pathogenesis of hypoplastic left heart syndrome (HLHS) [46]. Furthermore, a remarkable recovery of heart function in children with DCM, myocarditis [47,48] and myocardial infarction [49] is observed in a subset of patients during follow-up and a positive outcome may be influenced by stress tolerance of immature cardiomyocytes. The latter might also be involved in the regenerative capacity of the embryonic and neonatal mammalian heart after myocardial injury [50]. Although regeneration is primarily attributed to proliferation of uninjured cardiomyocytes, survival of cardiomyocytes in the area at risk might also contribute, either by reducing the overall extent of injury, by functional recovery of cells after the insult or by inducing proliferation of neighboring healthy cardiomyocytes. Whether the stress tolerance of immature cardiomyocytes can somehow be reactivated after terminal differentiation might be a key question when aiming to improve cardioprotective strategies in the adult heart. Interestingly, cellular stress response and mitochondrial quality control have been proposed to contribute to adult heart regeneration beyond cardiomyocyte renewal [51].

Funding

This research did not receive any specific grant from funding agencies in the public, commercial, or not-for-profit sectors but was supported by institutional funds of the Justus Liebig University Gießen and the University Hospital Münster.

CRediT authorship contribution statement

Nina Schraps: Formal analysis, Investigation, Visualization. **Michaela Tirre:** Investigation, Visualization. **Simon Pyschny:** Investigation, Visualization. **Anna Reis:** Methodology, Resources. **Hannah Schlierbach:** Methodology, Resources. **Matthias Seidl:** Methodology, Resources, Writing – review & editing. **Hans-Gerd Kehl:** Funding acquisition. **Anne Schänzer:** Investigation, Methodology, Writing – review & editing. **Jacqueline Heger:** Methodology, Resources, Writing – review & editing. **Christian Jux:** Funding acquisition, Supervision, Writing – review & editing. **Jörg-Detlef Drenckhahn:** Conceptualization, Formal analysis, Project administration, Supervision, Visualization, Writing – original draft.

Declaration of competing interest

The authors declare that they have no known competing financial

interests or personal relationships that could have appeared to influence the work reported in this paper.

Acknowledgements

We thank Ebru Erdogan, Janina Sommer and Jamie-Lee Sauer (Department of Pediatric Cardiology, Justus Liebig University Gießen) for technical assistance.

Appendix A. Supplementary data

Supplementary data to this article can be found online at https://doi.org/10.1016/j.freeradbiomed.2024.01.034.

References

[1] D. Ramaccini, V. Montoya-Uribe, F.J. Aan, L. Modesti, Y. Potes, M.R. Wieckowski, I. Krga, M. Glibetić, P. Pinton, C. Giorgi, M.L. Matter, Mitochondrial function and dysfunction in dilated cardiomyopathy, Front. Cell Dev. Biol. 8 (2021) 624216, https://doi.org/10.3389/fcell.2020.624216.

[2] B. Zhou, R. Tian, Mitochondrial dysfunction in pathophysiology of heart failure, J. Clin. Invest. 128 (2018) 3716–3726, https://doi.org/10.1172/JCI120849.

[3] E. Murphy, J.C. Liu, Mitochondrial calcium and reactive oxygen species in cardiovascular disease, Cardiovasc. Res. 119 (2023) 1105–1116, https://doi.org/10.1093/cvr/cvac134.

[4] G. Maroli, T. Braun, The long and winding road of cardiomyocyte maturation, Cardiovasc. Res. 117 (2021) 712–726, https://doi.org/10.1093/cvr/cvaa159.

[5] M. Sánchez-Díaz, J.Á. Nicolás-Ávila, M.D. Cordero, A. Hidalgo, Mitochondrial adaptations in the growing heart, Trends Endocrinol. Metabol. 31 (2020) 308–319, https://doi.org/10.1016/j.tem.2020.01.006.

[6] J.C. Garbern, R.T. Lee, Mitochondria and metabolic transitions in cardiomyocytes: lessons from development for stem cell-derived cardiomyocytes, Stem Cell Res. Ther. 12 (2021) 177, https://doi.org/10.1186/s13287-021-02252-6.

[7] B.N. Puente, W. Kimura, S.A. Muralidhar, J. Moon, J.F. Amatruda, K.L. Phelps, D. Grinsfelder, B.A. Rothermel, R. Chen, J.A. Garcia, C.X. Santos, S. Thet, E. Mori, M.T. Kinter, P.M. Rindler, S. Zacchigna, S. Mukherjee, D.J. Chen, A.I. Mahmoud, M. Giacca, P.S. Rabinovitch, A. Aroumougame, A.M. Shah, L.I. Szweda, H.A. Sadek, The oxygen-rich postnatal environment induces cardiomyocyte cell-cycle arrest through DNA damage response, Cell 157 (2014) 565–579, https://doi.org/10.1016/j.cell.2014.03.032.

[8] Y.R. Chen, J.L. Zweier, Cardiac mitochondria and reactive oxygen species generation, Circ. Res. 114 (2014) 524–537, https://doi.org/10.1161/CIRCRESAHA.114.300559.

[9] R.H. Henning, B.J.J.M. Brundel, Proteostasis in cardiac health and disease, Nat. Rev. Cardiol. 14 (2017) 637–653, https://doi.org/10.1038/nrcardio.2017.89.

[10] Z.V. Wang, J.A. Hill, Protein quality control and metabolism: bidirectional control in the heart, Cell Metabol. 21 (2015) 215–226, https://doi.org/10.1016/j.cmet.2015.01.016.

[11] K. Pakos-Zebrucka, I. Koryga, K. Mnich, M. Ljujic, A. Samali, A.M. Gorman, The integrated stress response, EMBO Rep. 17 (2016) 1374–1395, https://doi.org/10.15252/embr.201642195.

[12] R. Gomez-Pastor, E.T. Burchfiel, D.J. Thiele, Regulation of heat shock transcription factors and their roles in physiology and disease, Nat. Rev. Mol. Cell Biol. 19 (2018) 4–19, https://doi.org/10.1038/nrm.2017.73.

[13] X.G. Lei, J.H. Zhu, W.H. Cheng, Y. Bao, Y.S. Ho, A.R. Reddi, A. Holmgren, E. S. Arnér, Paradoxical roles of antioxidant enzymes: basic mechanisms and health implications, Physiol. Rev. 96 (2016) 307–364, https://doi.org/10.1152/physrev.00010.2014.

[14] N. Laforgia, A. Di Mauro, G. Favia Guarnieri, D. Varvara, L. De Cosmo, R. Panza, M. Capozza, M.E. Baldassarre, N. Resta, The role of oxidative stress in the pathomechanism of congenital malformations, Oxid. Med. Cell. Longev. 2018 (2018) 7404082, https://doi.org/10.1155/2018/7404082.

[15] C.J.A. Ramachandra, S. Hernandez-Resendiz, G.E. Crespo-Avilan, Y.H. Lin, D. J. Hausenloy, Mitochondria in acute myocardial infarction and cardioprotection, EBioMedicine 57 (2020) 102884, https://doi.org/10.1016/j.ebiom.2020.102884.

[16] M. Cardoso-Moreira, J. Halbert, D. Valloton, B. Velten, C. Chen, Y. Shao, A. Liechti, K. Ascenção, C. Rummel, S. Ovchinnikova, P.V. Mazin, I. Xenarios, K. Harshman, M. Mort, D.N. Cooper, C. Sandi, M.J. Soares, P.G. Ferreira, S. Afonso, M. Carneiro, J.M.A. Turner, J.L. VandeBerg, A. Fallahshahroudi, P. Jensen, R. Behr, S. Lisgo, S. Lindsay, P. Khaitovich, W. Huber, J. Baker, S. Anders, Y.E. Zhang, H. Kaessmann, Gene expression across mammalian organ development, Nature 571 (2019) 505–509, https://doi.org/10.1038/s41586-019-1338-5.

[17] M. Magarin, T. Pohl, A. Lill, H. Schulz, F. Blaschke, A. Heuser, L. Thierfelder, S. Donath, J.D. Drenckhahn, Embryonic cardiomyocytes can orchestrate various cell protective mechanisms to survive mitochondrial stress, J. Mol. Cell. Cardiol. 97 (2016) 1–14, https://doi.org/10.1016/j.yjmcc.2016.04.007.

[18] B. Grün, M. Tirre, S. Pyschny, V. Singh, H.G. Kehl, C. Jux, J.D. Drenckhahn, Inhibition of mitochondrial respiration has fundamentally different effects on proliferation, cell survival and stress response in immature versus differentiated cardiomyocyte cell lines, Front. Cell Dev. Biol. 10 (2022) 1011639, https://doi.org/10.3389/fcell.2022.1011639.

[19] C.J. Fiorese, A.M. Schulz, Y.F. Lin, N. Rosin, M.W. Pellegrino, C.M. Haynes, The transcription factor ATF5 mediates a mammalian mitochondrial UPR, Curr. Biol. 26 (2016) 2037–2043, https://doi.org/10.1016/j.cub.2016.06.002.

[20] J.E. Aldridge, T. Horibe, N.J. Hoogenraad, Discovery of genes activated by the mitochondrial unfolded protein response (mtUPR) and cognate promoter elements, PLoS One 2 (2007) e874, https://doi.org/10.1371/journal.pone.0000874.

[21] K.R. Bhattarai, T.A. Riaz, H.R. Kim, H.J. Chae, The aftermath of the interplay between the endoplasmic reticulum stress response and redox signaling, Exp. Mol. Med. 53 (2021) 151–167, https://doi.org/10.1038/s12276-021-00560-8.

[22] M. Chiong, Z.V. Wang, Z. Pedrozo, D.J. Cao, R. Troncoso, M. Ibacache, A. Criollo, A. Nemchenko, J.A. Hill, S. Lavandero, Cardiomyocyte death: mechanisms and translational implications, Cell Death Dis. 2 (2011) e244, https://doi.org/10.1038/cddis.2011.130.

[23] J. Ritterhoff, R. Tian, Metabolic mechanisms in physiological and pathological cardiac hypertrophy: new paradigms and challenges, Nat. Rev. Cardiol. 20 (2023) 812–829, https://doi.org/10.1038/s41569-023-00887-x.

[24] D.E. Place, P. Samir, R.S. Malireddi, T.D. Kanneganti, Integrated stress response restricts macrophage necroptosis, Life Sci. Alliance 5 (2021) e202101260, https://doi.org/10.26508/lsa.202101260.

[25] Y. Zou, W. Zhu, M. Sakamoto, Y. Qin, H. Akazawa, H. Toko, M. Mizukami, N. Takeda, T. Minamino, H. Takano, T. Nagai, A. Nakai, I. Komuro, Heat shock transcription factor 1 protects cardiomyocytes from ischemia/reperfusion injury, Circulation 108 (2003) 3024–3030, https://doi.org/10.1161/01.CIR.0000101923.54751.77.

[26] R. Romero-Becerra, A.M. Santamans, C. Folgueira, G. Sabio, p38 MAPK pathway in the heart: new insights in health and disease, Int. J. Mol. Sci. 21 (2020) 7412, https://doi.org/10.3390/ijms21197412.

[27] R.A. Kaiser, O.F. Bueno, D.J. Lips, P.A. Doevendans, F. Jones, T.F. Kimball, J. D. Molkentin, Targeted inhibition of p38 mitogen-activated protein kinase antagonizes cardiac injury and cell death following ischemia-reperfusion in vivo, J. Biol. Chem. 279 (2004) 15524–15530, https://doi.org/10.1074/jbc.M313717200.

[28] Q.M. Chen, A.J. Maltagliati, Nrf2 at the heart of oxidative stress and cardiac protection, Physiol. Genom. 50 (2018) 77–97, https://doi.org/10.1152/physiolgenomics.00041.2017.

[29] M.D. Brand, Mitochondrial generation of superoxide and hydrogen peroxide as the source of mitochondrial redox signaling, Free Radic. Biol. Med. 100 (2016) 14–31, https://doi.org/10.1016/j.freeradbiomed.2016.04.001.

[30] S. Dey, A. Sidor, B. O'Rourke, Compartment-specific control of reactive oxygen species scavenging by antioxidant pathway enzymes, J. Biol. Chem. 291 (2016) 11185–11197, https://doi.org/10.1074/jbc.M116.726968.

[31] L. Formentini, M. Sánchez-Aragó, L. Sánchez-Cenizo, J.M. Cuezva, The mitochondrial ATPase inhibitory factor 1 triggers a ROS-mediated retrograde prosurvival and proliferative response, Mol. Cell 45 (2012) 731–742, https://doi.org/10.1016/j.molcel.2012.01.008.

[32] S.H. Woo, J.C. Kim, N. Eslenur, T.N. Trinh, L.N.H. Do, Modulations of cardiac functions and pathogenesis by reactive oxygen species and natural antioxidants, Antioxidants 10 (2021) 760, https://doi.org/10.3390/antiox10050760.

[33] N. Momtahan, C.O. Crosby, J. Zoldan, The role of reactive oxygen species in in vitro cardiac maturation, Trends Mol. Med. 25 (2019) 482–493, https://doi.org/10.1016/j.molmed.2019.04.005.

[34] J.R. Hom, R.A. Quintanilla, D.L. Hoffman, K.L. de Mesy Bentley, J.D. Molkentin, S. S. Sheu, G.A. Porter Jr., The permeability transition pore controls cardiac mitochondrial maturation and myocyte differentiation, Dev. Cell 21 (2011) 469–478, https://doi.org/10.1016/j.devcel.2011.08.008.

[35] D. Zhang, Y. Li, D. Heims-Waldron, V. Bezzerides, S. Guatimosim, Y. Guo, F. Gu, P. Zhou, Z. Lin, Q. Ma, J. Liu, D.Z. Wang, W.T. Pu, Mitochondrial cardiomyopathy caused by elevated reactive oxygen species and impaired cardiomyocyte proliferation, Circ. Res. 122 (2018) 74–87, https://doi.org/10.1161/CIRCRESAHA.117.311349.

[36] S.F. Steinberg, Oxidative stress and sarcomeric proteins, Circ. Res. 112 (2013) 393–405, https://doi.org/10.1161/CIRCRESAHA.111.300496.

[37] G.W. Dorn 2nd, R.N. Kitsis, The mitochondrial dynamism-mitophagy-cell death interactome: multiple roles performed by members of a mitochondrial molecular ensemble, Circ. Res. 116 (1) (2015 Jan 2) 167–182, https://doi.org/10.1161/CIRCRESAHA.116.303554.

[38] A. Li, M. Gao, W. Jiang, Y. Qin, G. Gong, Mitochondrial dynamics in adult cardiomyocytes and heart diseases, Front. Cell Dev. Biol. 8 (2020) 584800, https://doi.org/10.3389/fcell.2020.584800.

[39] T. Kleele, T. Rey, J. Winter, S. Zaganelli, D. Mahecic, H. Perreten Lambert, F. P. Ruberto, M. Nemir, T. Wai, T. Pedrazzini, S. Manley, Distinct fission signatures predict mitochondrial degradation or biogenesis, Nature 593 (2021) 435–439, https://doi.org/10.1038/s41586-021-03510-6.

[40] E.Q. Toyama, S. Herzig, J. Courchet, T.L. Lewis Jr., O.C. Losón, K. Hellberg, N. P. Young, H. Chen, F. Polleux, D.C. Chan, R.J. Shaw, AMP-activated protein kinase mediates mitochondrial fission in response to energy stress, Science 351 (2016) 275–281, https://doi.org/10.1126/science.aab4138.

[41] A.P. Leonard, R.B. Cameron, J.L. Speiser, B.J. Wolf, Y.K. Peterson, R. G. Schnellmann, C.C. Beeson, B. Rohrer, Quantitative analysis of mitochondrial morphology and membrane potential in living cells using high-content imaging, machine learning, and morphological binning, Biochim. Biophys. Acta 1853 (2015) 348–360, https://doi.org/10.1016/j.bbamcr.2014.11.002.

[42] J.A. Ronchi, T.R. Figueira, F.G. Ravagnani, H.C. Oliveira, A.E. Vercesi, R. F. Castilho, A spontaneous mutation in the nicotinamide nucleotide transhydrogenase gene of C57BL/6J mice results in mitochondrial redox

abnormalities, Free Radic. Biol. Med. 63 (2013) 446–456, https://doi.org/10.1016/j.freeradbiomed.2013.05.049.

[43] A.G. Nickel, A. von Hardenberg, M. Hohl, J.R. Löffler, M. Kohlhaas, J. Becker, J. C. Reil, A. Kazakov, J. Bonnekoh, M. Stadelmaier, S.L. Puhl, M. Wagner, I. Bogeski, S. Cortassa, R. Kappl, B. Pasieka, M. Lafontaine, C.R. Lancaster, T.S. Blacker, A. R. Hall, M.R. Duchen, L. Kästner, P. Lipp, T. Zeller, C. Müller, A. Knopp, U. Laufs, M. Böhm, M. Hoth, C. Maack, Reversal of mitochondrial transhydrogenase causes oxidative stress in heart failure, Cell Metabol. 22 (2015) 472–484, https://doi.org/10.1016/j.cmet.2015.07.008.

[44] L. Nicin, W.T. Abplanalp, A. Schänzer, A. Sprengel, D. John, H. Mellentin, L. Tombor, M. Keuper, E. Ullrich, K. Klingel, R.B. Dettmeyer, J. Hoffmann, H. Akintuerk, C. Jux, D. Schranz, A.M. Zeiher, S. Rupp, S. Dimmeler, Single nuclei sequencing reveals novel insights into the regulation of cellular signatures in children with dilated cardiomyopathy, Circulation 143 (2021) 1704–1719, https://doi.org/10.1161/CIRCULATIONAHA.120.051391.

[45] J.G. Coles, C. Boscarino, M. Takahashi, D. Grant, A. Chang, J. Ritter, X. Dai, C. Du, G. Musso, H. Yamabi, J. Goncalves, A.S. Kumar, J. Woodgett, H. Lu, G. Hannigan, Cardioprotective stress response in the human fetal heart, J. Thorac. Cardiovasc. Surg. 129 (2005) 1128–1136, https://doi.org/10.1016/j.jtcvs.2004.11.055.

[46] X. Xu, K. Jin, A.S. Bais, W. Zhu, H. Yagi, T.N. Feinstein, P.K. Nguyen, J. D. Criscione, X. Liu, G. Beutner, K.B. Karunakaran, K.S. Rao, H. He, P. Adams, C. K. Kuo, D. Kostka, G.S. Pryhuber, S. Shiva, M.K. Ganapathiraju, G.A. Porter Jr., J. I. Lin, B. Aronow, C.W. Lo, Uncompensated mitochondrial oxidative stress underlies heart failure in an iPSC-derived model of congenital heart disease, Cell Stem Cell 29 (2022) 840–855.e7, https://doi.org/10.1016/j.stem.2022.03.003.

[47] P.M. Alexander, P.E. Daubeney, A.W. Nugent, K.J. Lee, C. Turner, S.D. Colan, T. Robertson, A.M. Davis, J. Ramsay, R. Justo, G.F. Sholler, I. King, R. G. Weintraub, National Australian Childhood Cardiomyopathy Study. Long-term outcomes of dilated cardiomyopathy diagnosed during childhood: results from a national population-based study of childhood cardiomyopathy, Circulation 128 (2013) 2039–2046, https://doi.org/10.1161/CIRCULATIONAHA.113.002767.

[48] O. Miera, M. Germann, M.Y. Cho, J. Photiadis, E.M. Delmo Walter, R. Hetzer, F. Berger, K.R.L. Schmitt, Bridge to recovery in children on ventricular assist devices-protocol, predictors of recovery, and long-term follow-up, J. Heart Lung Transplant. 37 (2018) 1459–1466, https://doi.org/10.1016/j.healun.2018.08.005.

[49] B.J. Haubner, J. Schneider, U. Schweigmann, T. Schuetz, W. Dichtl, C. Velik-Salchner, J.I. Stein, J.M. Penninger, Functional recovery of a human neonatal heart after severe myocardial infarction, Circ. Res. 118 (2016) 216–221, https://doi.org/10.1161/CIRCRESAHA.115.307017.

[50] L. Rolland, C. Jopling, The multifaceted nature of endogenous cardiac regeneration, Front Cardiovasc Med 10 (2023) 1138485, https://doi.org/10.3389/fcvm.2023.1138485.

[51] J.P. Leach, T. Heallen, M. Zhang, M. Rahmani, Y. Morikawa, M.C. Hill, A. Segura, J.T. Willerson, J.F. Martin, Hippo pathway deficiency reverses systolic heart failure after infarction, Nature 550 (2017) 260–264, https://doi.org/10.1038/nature24045.